A Computer-Based Electro-Hydraulic Controller for a Dual-Sided Self-Loading Trailer

Mark Fahey

A Thesis
Submitted in Fulfilment
of the Requirements for the Degree of
Masters in Mechanical Engineering
in the
Department of Mechanical Engineering
University of Canterbury
Christchurch
New Zealand

1998

Abstract

The design of a proposed new mechanism for the self-loading of shipping containers onto truck-trailers is described. The mechanism possess a complex array of interconnected hydraulic cylinders and has the ability to load from either side of the trailer. The objective of the research was to design, build and control a half-scale working model of the proposed mechanism in order to determine whether or not the concept of the design could be realised.

The mechanical design, hydraulic circuit, and kinematic analysis for the half-scale model are discussed in prelude to the controller design. A combined feedforward/feedback control strategy driven by teleoperator rate commands was found to be an effective way to control the mechanism.

In conclusion, the research was successful. The design concept was proven to work, and the controller was shown to provide excellent tracking performance. Work is now continuing on the design and development of a full-sized prototype.

Acknowledgements

I would like to dedicate this work to my Grandfather, Jack Waddell, and thank him for fostering my practical ability from an early age.

There are numerous people I wish to thank for their help and support in completing this thesis. Thanks to my fiancée Fiona, for putting up with my enthusiasm and hours of absence. Thanks to my academic supervisor Dr. Chris Damaren, and my industrial mentor Dr. Ernst Hustedt, for so obligingly passing on their wealth of knowledge. Many thanks for the technical assistance provided by Mr. Andy Cree and the other technicians in the University of Canterbury's Mechanical Department, and for the support given by Hydraulic Specialities Ltd., in particular Mr. Kim Clarke.

I would also like to acknowledge the financial assistance of the Foundation for Research, Science and Technology, provided under GRIF contract RMT601.

Contents

List of Figures

List of Tables

Chapter 1

Introduction

This document outlines the work undertaken on the design of a computer-based electro-hydraulic controller for a dual-sided self loading trailer. This work was the topic of a Master of Engineering Degree at the University of Canterbury, New Zealand.

1.1 Project's Background

Given the economy's reliance on overseas trade and the accessibility of freight via the sea, the handling of shipping containers is common to the New Zealand transport industry. Internal distribution of the freight is by rail or truck, but whichever system is used, efficient handling is of great importance.

The efficiency of handling is greatly affected by resources for loading and unloading of the shipping containers. Although trucks are the most flexible method for distribution, they are often impeded by the inability to unload. As a solution to this problem, truck-trailers with self-loading mechanisms have been designed. An example of such a machine is shown in Figure 1.1. At present however, there exists a limitation on these mechanisms; they are only capable of loading from one side.

This limitation becomes apparent when the truck is forced to manoeuvre in a confined area, in order to load or unload the container. To improve efficiency of handling further, the optimum self-loading trailer (SLT) would have the ability to operate from either side.

This need was identified by Rod MacKenzie and Grant MacKenzie of Rod MacKenzie Trucks Specialists Ltd., Timaru. They proposed a more versatile design of mechanism which permitted dual-side loading. A partnership was formed between Rod MacKenzie Truck Specialists Ltd. and Advanced Mechanical Engineering Solutions (A.M.E.S.).

It was through A.M.E.S. that graduate mechanical engineering student, Mark Fahey became involved with the project. Given the proposed design, his task was to investigate the requirements of a electro-hydraulic controller. The heavy research and development nature of the project made it an ideal candidate for a Graduate Research in Industry Fellowship (GRIF) from the Foundation for Science, Research and Technology. Hence this aspect of the project became the topic of this thesis at the University of Canterbury.

Figure 1.1: Example of an Existing Self Loading Trailer Mechanism.

1.2 Businesses' Background

Rod MacKenzie Trucks Specialists Ltd. belongs to the Rod MacKenzie Group of Companies and employs 10 staff. They provide servicing and repairs to the heavy transport industry, lease a fleet of rental trucks, and are suppliers of 4 Wheel Drive parts. The SLT venture is not the first of its kind for the business, but it is probably the most ambitious. Rod MacKenzie Trucks has already successfully converted a standard 40 foot trailer into a custom tip trailer for coal delivery. A.M.E.S. was asked by Rod MacKenzie Truck Specialists Ltd. for aid with the mechanical design details.

Advanced Mechanical Engineering Solutions is a mechanical engineering consultancy business who specialise in design and computer simulation of mechanical systems. Using Finite Element Analysis software, the type of work undertaken by A.M.E.S. ranges from simulation of deep-sea pipe-lay operations, to stress, deformation and frequency analysis of water-jet propulsion units.

Dr. Ernst Hustedt, the principal of A.M.E.S. has undertaken the self-loading trailer project out of personal interest, and has been the industrial mentor for the purposes of the GRIF.

1.3 Proposed Market

Several hundred self-loading trailers are in operation in NZ at present. Market research indicates that there exists a niche market for a self-loading trailer with the capability of loading from either side, providing factors such as cost and tare weight make the new machine a comparable product to existing self-loading trailers.

The market is not entirely limited to NZ. Despite being the leaders internationally in the field, there has been interest in the proposed device from contacts in South-East Asia and the United Kingdom. The improved handling efficiency would make the dual-sided mechanisms attractive anywhere that space is at a premium.

1.4 Need for Computer Controlled Mechanism

Designing a practical mechanism for lifting full containers from either side of the self-loading trailer is by no means a straightforward task. This is confirmed by the fact that with the exception of one design, all the self-loading trailers in the international market are capable of loading from one side only. The one exception is a German design by *Klaus* which is in fact too heavy to be legal on New Zealand roads [1]. The proposed mechanism is a practical solution to the dual-side problem.

Due to the nature of the mechanism, its control is relatively complex. The need for computer control comes from the necessity to coordinate the motion of multiple hydraulic cylinders. As there are more actuators than there are degrees of freedom in the proposed mechanism, there exists the potential for the mechanism to become over-constrained and 'lock up'. It would be impossible for the operator to coordinate multiple cylinders manually, hence the purpose of the controller is to allow the operator to move the mechanism easily.

While it may be seen as undesirable to carry a computer on board a truck trailer, it allows for a 'smart' trailer with some substantial advantages. User-friendly operator controls can be employed, with automated loading and stow features, and pure horizontal and vertical motion control of the payload. It also allows load sensing to limit the safe working payload, maintain system integrity, and data logging to store information on the life history of the mechanism.

1.5 Scope of Master's Thesis

In order to aid the design of the prototype SLT and allow testing, it was decided to construct a half-scale model. This became the aim of the Masters degree: to design, build and control a half-scale working model of the proposed mechanism in order to determine whether the concept of the design could be realised.

1.6 Outline of this Document

This document discusses the concept and design of the half-scale model, followed by the design of the hydraulic circuit, the kinematic analysis, input/output (I/O) hardware and the controller design. Results from testing are presented and indicate the performance achieved by the controller.

Chapter 2

Design of Half-Scale Model

As the new concept provided no guarantee of working, a half-scale working model was designed and constructed. This allowed for testing and development with minimal financial risk.

2.1 Design Constraints

A number of constraints hinder the design solution of the dual-side SLT. The dimensions of the mechanism are constrained by law. The crane must stow behind a silhouette of the 2438 mm width and 2591 mm height for an ISO standard container. Length requirements dictate that the thickness of the mechanism be less than 700mm [2]. To prevent the trailer from tipping over when lifting, stabiliser legs are required. The stabiliser legs must be housed within the aforementioned space, along with the crane.

Admittedly, a single-sided SLT suffers from the same constraints, however the constraints impinge on the dual-sided mechanism more severely. The dual-sided mechanism requires more reach, as it must be located in the centre of the trailer for working either side. This is in contrast to the single-sided mechanism which can be located at the edge of the trailer closest to the container. The further the reach, the larger the lever arm and hence the greater the torque required for lifting a given load. Also the dual-sided mechanism requires a stabiliser leg for each side, compared with the single leg for single-sided operation. Essentially the main difficulty is fitting the mechanism into the legally confined space.

In arriving at a practical design, the mechanism must reach the required points in space. Furthermore, given the relatively large payload (in the order of 30 tonne), the design must minimise the forces required from the actuators. The maximum payload carried by the SLT is dependent on its tare weight; thus minimising tare weight is another objective.

The overall design constraint is financial. Tare weight can always be reduced, but the lighter the trailer becomes, the cost per kilogram of weight removed increases. The increased versatility of the dual-sided SLT requires more hydraulic cylinders and more materials than the single-sided version and therefore costs and weighs more. The financial constraints are offset somewhat by the improved operator controls and the other 'smart'

features that the proposed mechanism offers. At the end of the day however, the final product must be cost competitive, in order to capture a market share.

2.2 The Proposed Design

The proposed design (NZ Patent No. 286210) is shown in Figure 2.1. The mechanism has three moving joints. The arm on top, called the swing-arm, can pivot about the apex of the larger triangle. The larger triangle itself is attached to a mast. The mast is a sliding arrangement which can extend, and can also tilt about a pivot point at the base.

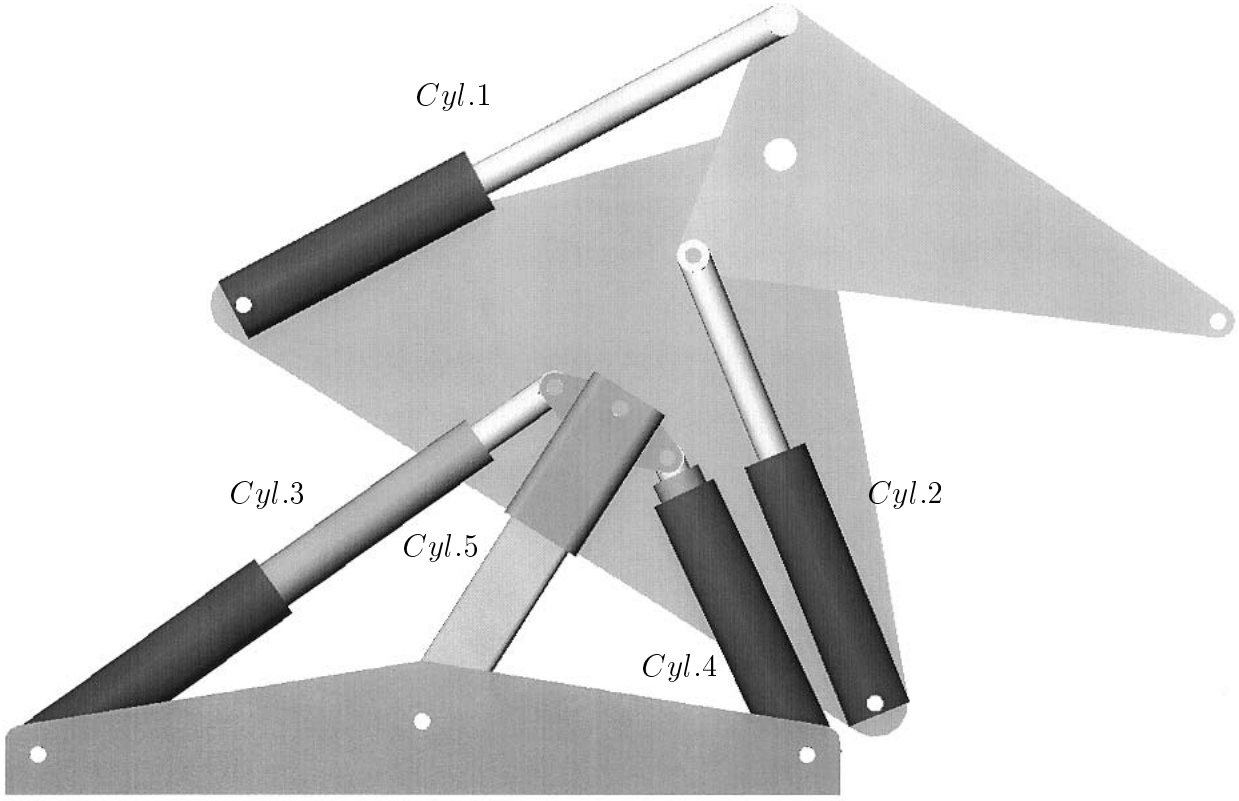

Figure 2.1: Proposed Mechanism.

Hydraulic cylinders 1 and 2 rotate the swing-arm about its pivot point. The angular position of the arm is defined by the variable α. For effective movement of the joint, the cylinders must move in unison. Failure to move in unison will cause excessive loading on the joint.

A similar situation exists with the cylinders actuating the tilt and extension of the mast. The reach off the side of the truck is achieved with telescopic side cylinders 3 and 4. These cylinders are single acting in compression. The tension force for supporting the load and retracting the telescopic cylinders is supplied by a another cylinder, cylinder 5, hidden inside the mast. As three cylinders are actuating only two degrees of freedom

(tilt, θ, and extension, χ, of the mast), again multiple cylinders must move synchronously to provide unrestricted joint movement.

The mechanism has the ability to load containers from either side, picking up the container from the ground or from another trailer alongside. The design also allows for the transfer of the container from one side to the other. The third potential pickup point is a container stacked two-high. This point is out of reach for the present design; however, modifications could possibly be made to reach this point.

The dimensions of the mechanism were selected after some preliminary modelling and optimisation with the finite element software ANSYS, and then with SolidWorks 97. SolidWorks 97 is solid modelling CAD software which allows solid, virtual models to be constructed and animated. The greatest advantage of SolidWorks 97 as a design tool for this application, is that it was fully parametric. This allowed every dimension that defined the model to be altered and the effect of the alteration on the mechanism's reach to be examined. This iterative procedure aimed to obtain maximum useful reach, while being able to stow behind the silhouette of the container.

The compactness of the mechanism depends a great deal on the design efficiency (that is ratio of open centre distance to closed centre distance) of the hydraulic cylinders. The dead-length built into the design of the hydraulic cylinders is for housing seals, wipers and linear bearing. Most of the dead-length is required to achieve sufficient distance between bearings. This prevents excessive bearing loads caused by non-axial forces and moments on the cylinder.

ANSYS was most useful for analysing the forces in the mechanism. Of particular interest were graphs which display the required force versus length for each hydraulic cylinder. With careful consideration of these graphs, hydraulic cylinders could be designed which minimise the dead-length but still provide sufficient dead-length for protection against failure by buckling. Thus the range of motion of the mechanism was maximised.

2.3 Purpose of Model

The primary purpose of the model is to simulate the kinematics of the full-sized mechanism. That is, to make the model move in a similar fashion to the full-sized prototype. Secondary purposes of the model are to aid the design of the hydraulic circuit, enable input/output (I/O) requirements to be determined, provide a trial for position and velocity sensing, and allow software design and a feedback control strategy to be investigated.

2.4 Design of Model

As Figure 2.2 shows, the design of the model was based on the concept for the full-sized prototype. At approximately half scale, it had the same joint movements, and rams in a similar configuration. The difference between the model and the intended full-sized design is the range of movement. To avoid the high cost of telescopic cylinders, single-stage cylinders had to suffice for the model. This does not affect the working principles,

but merely limits range. The student closely consulted with Ernst Hustedt of A.M.E.S. during the design of the model.

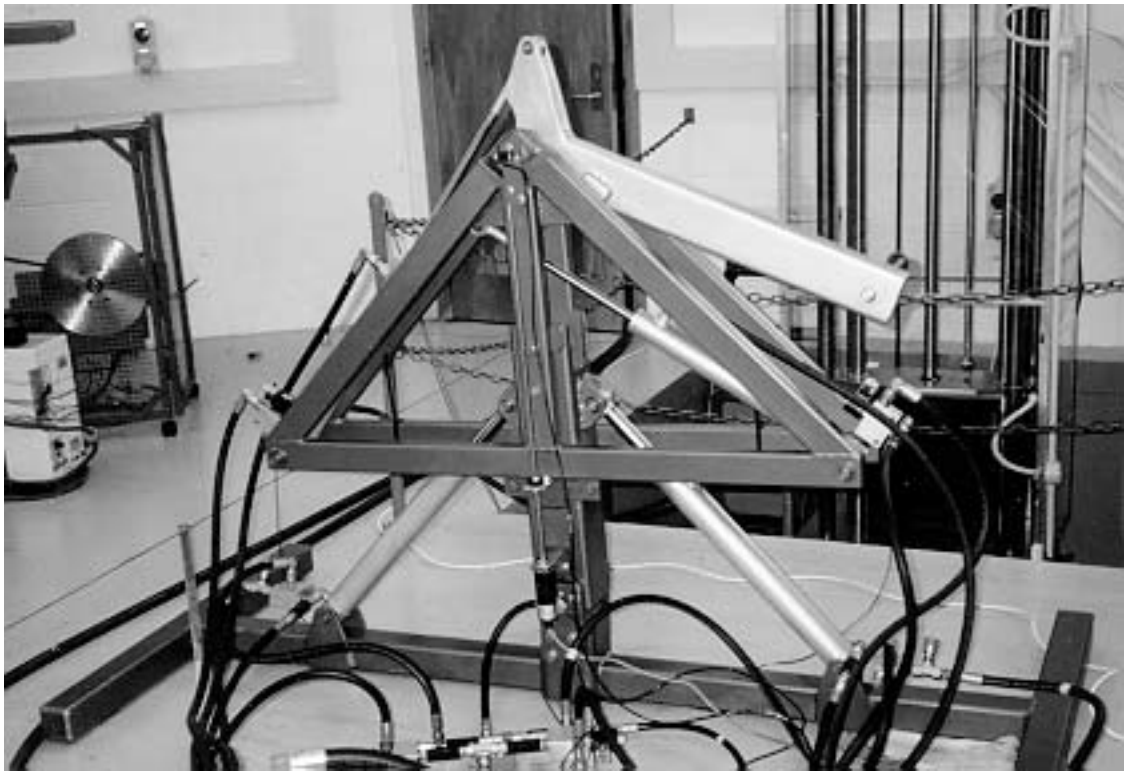

Figure 2.2: Photograph of Half-Scale Model.

The first detail to consider in the design of the half-scale model was the dimensioning of the hydraulic cylinders. The open and closed centre dimensions would determine the range of motion of the mechanism. Less important were the rod and cylinder diameters which, given pressure, determine the force that the actuator can produce. As the maximum payload carried by the model was not important in the model's purpose, and cylinders are manufactured in standard sizes, the selection of cylinder diameters was based on availability and attaining practical hydraulic flow rates. The cylinders were manufactured by Hydrapower Systems Ltd. to the specified dimensions shown in Table 2.1, and the range of movement the cylinders allowed the three joints of the mechanism α, θ and χ is displayed in Table 2.2.

Cylinder	Closed Centre	Open Centre	Cyl. Dia.	Rod. Dia
1	660 mm	1015 mm	1.5"	0.75"
2	660 mm	1015 mm	1.5"	0.75"
3	550 mm	960 mm	2.0"	1.25"
4	550 mm	960 mm	2.0"	1.25"
5	430 mm	730 mm	1.5"	0.75"

Table 2.1: Cylinder Dimensions in Model.

Joint	Minimum Position	Maximum Position
α	-118 degrees	+118 degrees
θ	-31 degrees	+31 degrees
χ	386 mm	690 mm

Table 2.2: Range of Movement of Model.

The hydraulic cylinders are designed to withstand 3000 psi (20.7 MPa) of continuous pressure. For the 1.5" $\times$ 0.75" cylinders which actuate the swing-arm, the force generated at this pressure in tension is 18 kN. The weakest swing-arm position is when one cylinder is singular, which means it has no leverage. At this position, the other, non-singular cylinder has 0.2 meter of leverage. Given that the leverage of the payload is 0.7 meters, the maximum payload that can be carried by the model is 515 kg.

Joint	Desired Maximum Joint Speed
α	15 degrees per second
θ	5 degrees per second
χ	30 mm per second

Table 2.3: Joint Velocities of Model.

From the desired joint velocities shown in Table 2.3, the flow rates of hydraulic oil required by the cylinders could be calculated. The cylinder velocities are configuration dependent for a given set of joint rates. Using the peak velocities, and knowing the cylinder cross-sectional area, the flow rate q can be calculated using:

$$q = VA \tag{2.1}$$

where V is the cylinder velocity and A is the piston area. Note that owing to the rod, the area is less for retraction than extension. The ensuing peak flow-rate requirements were calculated as given in Table 2.4

Cylinder	Peak Flow Rate Required
1	4.7 litres/minute
2	4.7 litres/minute
3	3.6 litres/minute
4	3.6 litres/minute

Table 2.4: Maximum Flow-Rates Required by Cylinder in Model.

For reasons discussed in the following chapter, the flow rate for cylinder 5, the tension cylinder hidden in the mast was not required. The flow rates required for extending the mast are in excess of the flow rates required for tilting it, and hence determine the peak flow rates for cylinders 3 and 4.

The structure of the model itself was designed as an assembly of square and rectangular hollow section steel and steel plate. Components were fabricated by welding and

then the assembly was bolted together upon a heavy base frame. Critical stress areas were identified and hand calculations ensured the strength of the design.

The design of the joints required particular attention. Ultra high molecular weight polyethylene or UHMPWE was used for both the linear and rotational bearings of the three joints. Couplings were designed for attaching sensors to measure the position of the joints.

Workshop drawings were produced (as shown in Appendix A) and the model was manufactured at Rod MacKenzie Truck Specialists Ltd. With the physical model built, the other aspects of the system could then be designed.

Chapter 3

Hydraulic Circuit Design

Hydraulic power is a universally accepted solution for heavy lifting applications of the nature being studied in this project. A circuit had to be designed to safely and effectively harness this power, and operate the mechanism in the desired manner.

3.1 Hydraulic Power-Pack

The hydraulic power originates from an electric motor and hydraulic pump. Electrical energy is converted to fluid pressure and flow.

The power requirements of the system were calculated based on the maximum system pressure of 3000 psi (20.7 MPa) and the sum of the required cylinder flow rates, 16.6 litres per minute, from Table 2.4. The power is given by

$$P = pQ \tag{3.1}$$

where P is the power required to generate the pressure, p, and flow, Q. The product of the pressure and flow values given above is 5.7 kW. A 10 horsepower (7.5 kW), 2 pole electric motor was selected for driving the hydraulic pump.

The hydraulic pump is a 16 cubic-centimeter per revolution gear pump. The face-plate of the electric motor was modified to fit a bell housing, which along with a flexible shaft coupling, were purchased to connect the pump and motor together. A frame was designed and built to carry the pump and motor, and support the reservoir. Synchronous speed for the 2 pole motor is 1440 rpm. At 16 cubic-centimeters per revolution, the output flow-rate of the pump is 23 litres per minute, sufficiently more than the 16.6 litres per minute (maximum) required by the model.

As the power-pack was to be located in a room adjacent to the Hydraulics Laboratory, the start/stop switch and an emergency stop switch were tethered by 20 meters of cable. A one inch diameter supply and return hoses connected the power-pack to the model with quick-release couplings. The oil returning to the reservoir was passed through a 10 micron filter to remove any particle contaminants. Also, a pressure relief valve was connected between the pump supply and return to prevent overloading of the system.

3.2 The Hydraulic Control Valve

Until more recent years, cost has prohibited the use of proportional electro-hydraulic valves in industry. Rather than have variable flow, it has been more common to opt for on/off type valves. However as manufacturing costs and the cost of electronics are decreasing, the advantages of soft start/stop and proportional flow is now being recognised. The amalgamation of smart technology with the strength of hydraulics has the potential to be a far-reaching combination.

There are however other difficulties associated with controlling hydraulics; the principle one being the nonlinear relationship between input, x_v, the movement of the flow control spool, and the output flow, q. Figure 3.1 shows the relationship between spool position, flow rate and cylinder velocity. Neglecting internal leakage across the lands of the spool, the relationship is given by

$$q = C_d w x_v \sqrt{\frac{2}{\rho}(p_S - p_L)} \tag{3.2}$$

where C_d is the coefficient of discharge of the metering orifice, w is the area gradient of the notch, ρ is the density of the hydraulic fluid, p_S is the pressure of the oil on the supply side of the spool and p_L is the pressure on the load side of the spool [3]. As p_L is not constant, the flow rate from the valve is dependent on the load.

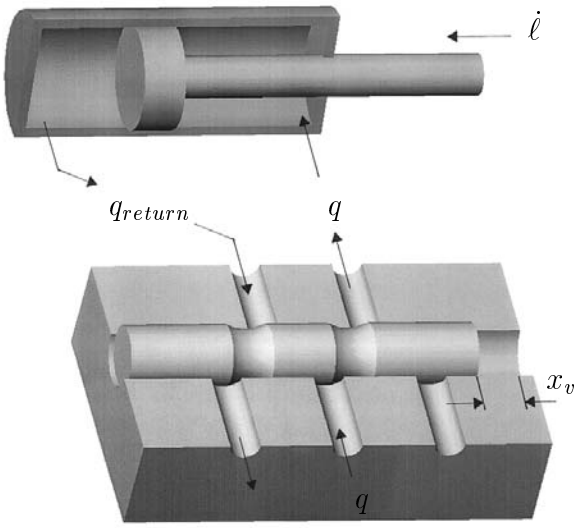

Figure 3.1: Path of Hydraulic Oil Through Control Valve.

A solution to this difficulty has been found by a United States hydraulic valve manufacturer called Apitech. The method employed by Apitech VPL series valve is to maintain a constant pressure drop across the flow control spool. This is done by sensing the pressure required by the load and regulating the supply pressure to be 200 psi greater than this value. This makes $(p_S - p_L)$ constant and therefore the output flow, q directly proportional to the input x_v.

3.2.1 Apitech VPL

The major influence in the decision to the purchase Apitech VPL series valve, as shown in Figure 3.2 was the lower cost when compared with other mobile proportional valves. The cost effectiveness is realized when multiple valves are required. The valve block is in modular form, with an inlet/outlet section, the number of valve sections required and an end section. Up to 12 valves can be incorporated in one block, and each valve operates independently of the others.

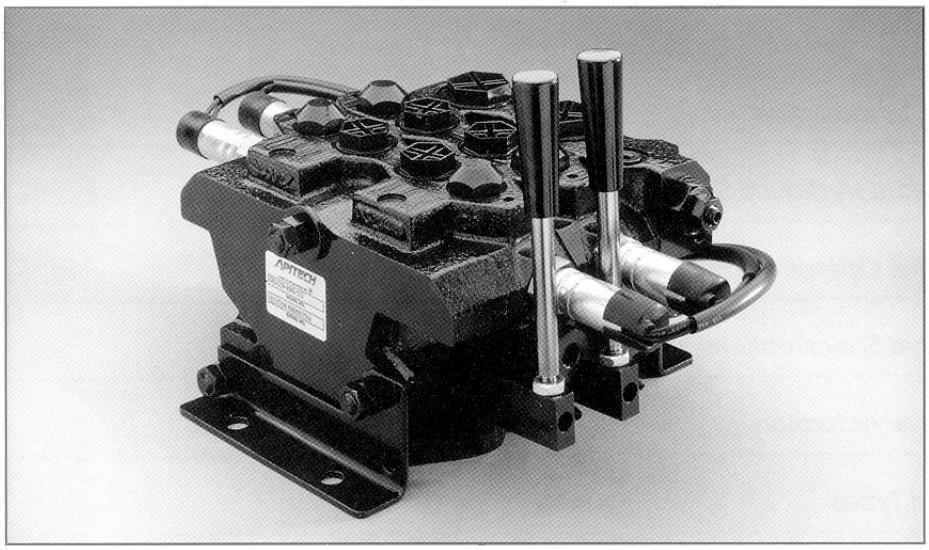

Figure 3.2: APITECH VPL Series Valve.

Electrical control of the VPL series valve is achieved with the Pulsar electro-hydraulic pilot valve. The Pulsar is driven with a digital pulse width modulated signal, being driven on and off at 33 Hz. This is far higher than the 2 Hz frequency response of the flow control spool, and keeps the spool displaced. The pulses serve to keep the spool from the grip of static friction, resulting in excellent linearity and low hysteresis. Combined with the load sensing which makes the valve independent of pressure, the valve is very controllable.

Yet another feature of the VPL valve is its versatility. It will allow various proportional maximum output flows to the cylinder ports; even allow a different maximum output flow to each port of the same valve. Cavity plugs can be added to provide shock and suction protection for the cylinder, and the ports can be individually pressure limited.

3.3 The Hydraulic Circuit

A hydraulic circuit was designed to make the system work more effectively, and also provide a standard safety requirement with counter-balance valves. A copy of the final circuit can be found in Appendix B.

3.3.1 Mast Subsystem

The difficulty with having more actuators than degrees of freedom, is that multiple cylinders must move synchronously. Failure to move in such a way as to satisfy the kinematical constraints will cause the mechanism to 'lock up'. The original strategy was to control each cylinder individually with its own proportional valve, however the precision that this method would require meant that an alternative solution had to be found.

The alternative solution applied mainly to the lower three cylinders (cylinders 3, 4 and 5 shown in Figure 2.1) which actuate the tilt and extension of the mast. In the full-sized mechanism, the outer two cylinders, cylinders 3 and 4, are two-stage telescopic. For economic and practical reasons, these are single acting in extension only. That is, they cannot retract themselves or hold a tensile load. The function of cylinder 5 is to carry the tensile load and provide the retraction function for the telescopic side cylinders.

The breakthrough came when a hydraulic circuit design was found, which allowed the tension cylinder to be slaved to the telescopic cylinders. The tension cylinder could be shared by the telescopic cylinders simultaneously or individually, as required. It eliminated the need for the VPL valve section used to control the tension cylinder, and bought the number of control inputs for the mast subsystem down to two, equaling the number of degrees of freedom.

The extension function of cylinders 3 and 4 is achieved by applying pressure to the piston side of either or both cylinders, and allowing oil to leave cylinder 5. Alternatively, cylinders 3 or 4 are retracted by feeding oil into cylinder 5. Cylinders 3 and 4 can move individually or simultaneously in either direction. In the case where one cylinder is extending and the other is retracting, a solenoid-operated check-valve is energised to prevent the extending cylinder from over-riding the retracting cylinder. The circuit which achieves this can be found in Appendix B.3.

The other advantage of this design is that it eliminates problems associated with the load passing 'over centre', and the consequential load transfer from one telescopic side cylinder to the other. From a static force perspective, the system is in equilibrium in any geometric configuration, while from the controllers perspective, the tension (or mast) cylinder is invisible. This allows the telescopic side cylinders to be extended or retracted as though they were double acting.

3.3.2 Swing Arm Subsystem

As the swing arm system has two cylinders for its one degree of freedom (cylinders 1 and 2 shown in Figure 2.1), there is potential for it also to become over-constrained . The cylinders act in a similar fashion to pistons in a reciprocating engine, translating linear motion into rotation of the swing arm joint.

The critical region is when the cylinder must pass through bottom dead centre. At this point, the direction of motion changes and hence the controller must supply pressure to the other side of the piston. As the VPL valve is relatively slow, there is a difficulty in getting the timing of this event correct.

To overcome this problem, a circuit was designed which allowed the cylinder to

be temporarily 'floated' through this critical region, while the required force for motion was supplied by the other cylinder. A solenoid operated valve opened both ends of the appropriate cylinder to tank. Thus pressure could not be applied to the wrong piston face.

3.3.3 Counter-Balance Valves

To comply with safety requirements, the circuit requires the use of counter-balance valves. These protect against a hose breaking or a hydraulic component failing. Counter-balance valves are mounted on the cylinder itself and prevent the cylinder from moving unless a pilot pressure signal to the counter-balance valve allows it to do so. This setup also protects against the load from running away under the influence of gravity and has a relief function for limiting the maximum cylinder pressure. Hence safety is an inherent feature of the circuit.

3.4 Practical Implementation of Hydraulic Circuit

A vast amount has been learned during the practical implementation of the hydraulic circuit. Some major difficulties were encountered in trying to find the cause of a shuddering when the hydraulics were operated. Despite being a relatively simple circuit, the interplay between the various functions made for difficult trouble-shooting.

Originally air was thought to be the problem. There are a number of ways air can enter the hydraulic system, and once in there, it finds its way to the highest point. Often it is flushed through, but sometimes it can become trapped. It is noticeable by its compressibility. Oil entering the cylinder compresses the air before moving the piston. Once the pressure against the piston overcomes the static friction of the seals, the piston jumps forward, decompressing the air. The cycle repeats and is witnessed by a jerky extension of the cylinder.

Air was diagnosed for two reasons. The first was that air was visibly being drawn into the pump. There was not enough oil covering the pump inlet filter and a spiral of air bubbles could be seen travelling downwards. The second reason was that air was being ejected in a spluttering stream of oil when the plug was removed from the load sensing port of the VPL valve.

All possible air leaks in the system were checked. The inlet filter was removed lest the restriction be causing a vacuum at the pump inlet; hose clamps were replaced and tightened; the dry side of the single-acting cylinders was checked in case air was being drawn past the piston seals; even the pump was replaced due to the age of the original pump and the chance that the seals were leaking.

The confusing factor was the intermittent nature of the problem. An adjustment would appear to fix the problem, only to have it reappear a time later. When air could no longer be put to blame, other things were considered, such as a faulty inlet compensator in the VPL valve. It took quite sometime before the real cause was unearthed.

One unusual factor was the excessive pressure required to retract cylinders 3 and 4. It was found that the flow from the piston side of these cylinders returning to tank

was greatly in excess of the flow entering the rod side of the tension cylinder, cylinder 5. The unequal flows were causing the return flow through the valve to be restricted. This factor was compounded by size differences between cylinders 3 and 4, and cylinder 5, and also the geometry of the mechanism. The pressure was being relieved by the tension cylinder's counter-balance valve. By giving the returning oil a direct line to tank, the problem was remedied.

However, it was found that the same symptoms were observed if the flow leaving the cylinder was too unrestricted. In this case when retracting cylinders 3 or 4, without sufficient back-pressure the cylinders would collapse under gravity. This causes the pilot pressure to drop and the counter-balance valve to close. Needle valves were used to provide the correct degree of restriction on the flow leaving the cylinder. A better solution still, is to provide back-pressure with lightly-set relief valves. This provides a restriction that is independent of flow.

Chapter 4

Kinematical Analysis

Kinematical analysis is the description of motion, the purpose of which is to provide the mathematical link between joint motion and cylinder motion.

4.1 Overview of Kinematical Analysis of Mechanism

At any time the hydraulic cylinders have a length and velocity. This information is described in 'ram' or ℓ-space. Likewise, information pertaining to the three joints, is described in 'joint' or ρ-space. By definition, the mapping from ram space to joint space is the forward solution. Conversely mapping from joint space to ram space is the inverse solution. Figure 4.1 defines the variables which will be used in this analysis.

4.2 Swing-Arm Mechanism

First, the swing-arm mechanism was considered. The swing-arm mechanism has two cylinders which actuate the rotational swing-arm joint. The first step in the analysis was to find the relationship between the ram lengths and the joint angle. The general mechanism was considered and the cosine rule was used to find the cylinder lengths (ℓ_1, ℓ_2) as a function of the joint position, α. These relationships are:

$$\ell_1(\alpha) = \sqrt{(r^2 + c^2) - 2rc\cos(\pi/2 - \gamma + \sigma + \alpha)} \tag{4.1}$$

$$\ell_2(\alpha) = \sqrt{(r^2 + c^2) - 2rc\cos(\pi/2 - \gamma + \sigma - \alpha)} \tag{4.2}$$

As is expected, ℓ_1 and ℓ_2 are independent of the position of the other two joints, θ and χ.

Eqs. (4.1) and (4.2) relate position information from joint space to ram space. As the operator commands joint motion, and the hydraulic valves regulate cylinder velocity, the controller also requires that velocity information be mapped. The result of differentiating Eq. (4.1) with respect to time gives,

$$\dot{\ell}_1 = J_{11}(\alpha)\,\dot{\alpha}, \quad J_{11} = \frac{rc\sin(\pi/2 - \gamma + \sigma + \alpha)}{\ell_1} \tag{4.3}$$

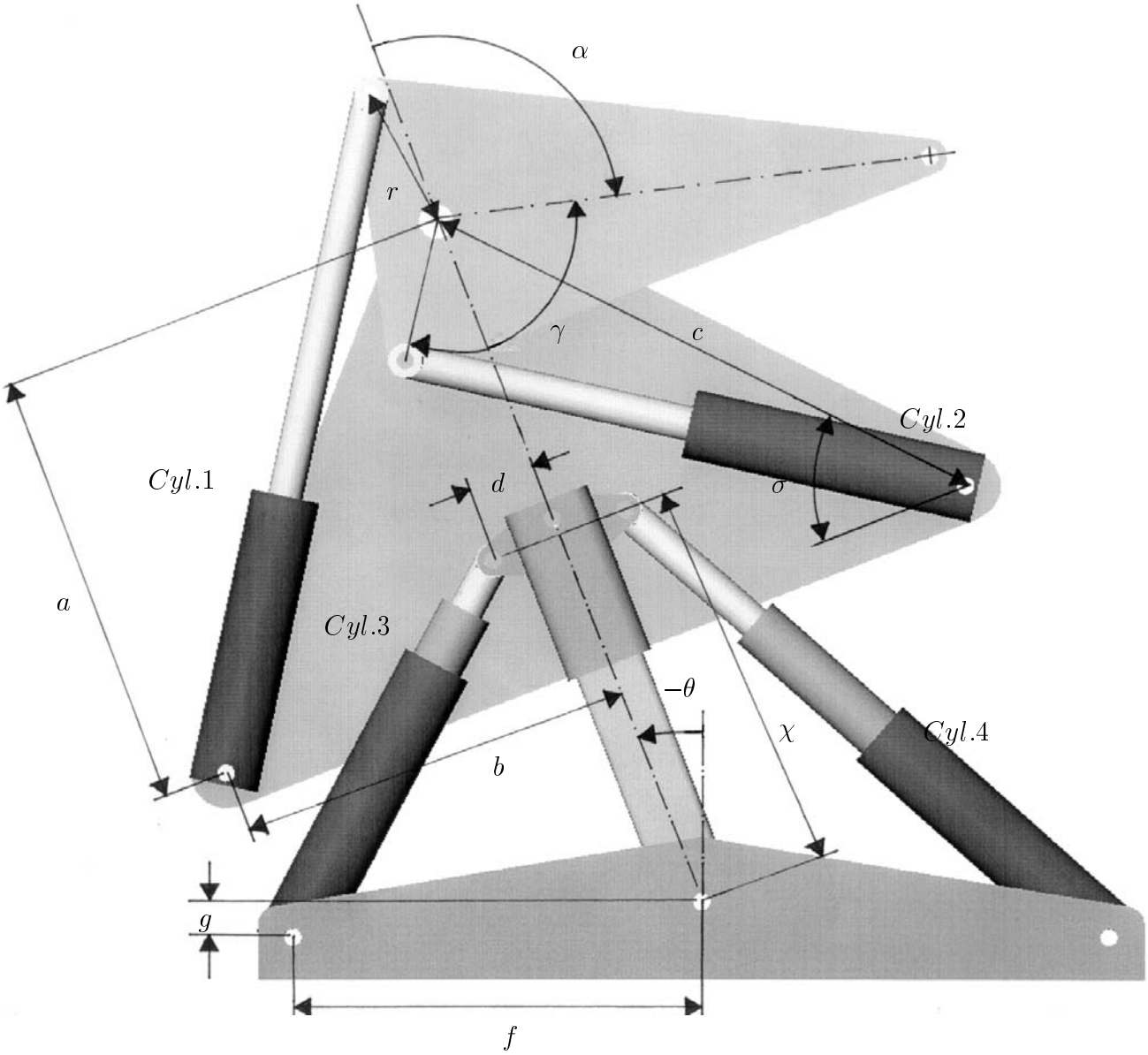

Figure 4.1: Description of Variables used for Kinematic Analysis.

The same operation performed on Eq. (4.2) yields a similar result:

$$\dot{\ell}_2 = J_{21}(\alpha)\,\dot{\alpha}, \quad J_{21} = \frac{rc\sin(\pi - \gamma + \sigma - \alpha)}{\ell_2} \tag{4.4}$$

The meaning of the subscripts on the symbol J will become clear.

Being a parallel-type robotic system, the inverse solution is more easily found than the forward solution. This is in contrast to a serial-type system where the forward solution is more natural. The other interesting characteristic of the swing-arm system, is that there are two solutions to the forward problem, one given by each cylinder. As the sensors on the model SLT mechanism provides information about the joint, it is the inverse solution which is required by the controller.

4.3 Mast Mechanism

The same procedure was performed on the two remaining degrees of freedom: the tilt (θ) and extension (χ) joints of the mast. As the hydraulic circuit design eliminates the need to control the tension cylinder, only the two telescopic cylinders had to be considered in the analysis.

The relationship between the cylinder lengths and the joint positions were again found with the cosine rule:

$$\ell_3(\theta,\chi) = \sqrt{(\chi^2 + d^2 + f^2 + g^2) - 2\sqrt{\chi^2 + d^2}\sqrt{f^2 + g^2}\sin\phi} \tag{4.5}$$

where $\phi = -\theta + \arctan(d/\chi) - \beta$, $\beta = atan(g/f)$, and

$$\ell_4(\theta,\chi) = \sqrt{(\chi^2 + d^2 + f^2 + g^2) - 2\sqrt{\chi^2 + d^2}\sqrt{f^2 + g^2}\sin\psi)} \tag{4.6}$$

where $\psi = \theta + \arctan(d/\chi) - \beta$.

Eqs. (4.5) and (4.6) were differentiated with respect to time to yield the following mappings from joint velocities to cylinder velocities:

$$\dot{\ell_3} = J_{32}\dot{\theta} + J_{33}\dot{\chi} \tag{4.7}$$

$$\dot{\ell_4} = J_{42}\dot{\theta} + J_{43}\dot{\chi} \tag{4.8}$$

where

$$J_{32} = \frac{1}{\ell_3}\left[\sqrt{g^2 + f^2}\sqrt{\chi^2 + d^2}\cos\phi\right]$$

$$J_{42} = \frac{1}{\ell_4}\left[\sqrt{g^2 + f^2}\sqrt{\chi^2 + d^2}\cos\psi\right]$$

$$J_{33} = \frac{1}{\ell_3}\left[\chi - \frac{\sqrt{g^2 + f^2}(\chi\sin\phi - d\cos\phi)}{\sqrt{\chi^2 + d^2}}\right]$$

$$J_{43} = \frac{1}{\ell_4}\left[\chi - \frac{\sqrt{g^2 + f^2}(\chi\sin\psi - d\cos\psi)}{\sqrt{\chi^2 + d^2}}\right]$$

4.4 Assembly of the Jacobian Matrix

The (inverse) Jacobian can be extracted from Eqs. (4.3), (4.4), (4.7) and (4.8), yielding a more concise expression for the joint velocity to cylinder velocity transformation. Given the positions ($\boldsymbol{\rho}$) and velocities ($\dot{\boldsymbol{\rho}}$) of the joints, the rate of extension of the cylinders ($\dot{\boldsymbol{\ell}}$) can be calculated using

$$\begin{bmatrix} \dot{\ell_1} \\ \dot{\ell_2} \\ \dot{\ell_3} \\ \dot{\ell_4} \end{bmatrix} = \begin{bmatrix} J_{11} & 0 & 0 \\ J_{21} & 0 & 0 \\ 0 & J_{32} & J_{33} \\ 0 & J_{42} & J_{43} \end{bmatrix} \begin{bmatrix} \dot{\alpha} \\ \dot{\theta} \\ \dot{\chi} \end{bmatrix} \tag{4.9}$$

or simply,

$$\dot{\boldsymbol{\ell}} = \mathbf{J}(\boldsymbol{\rho})\,\dot{\boldsymbol{\rho}} \tag{4.10}$$

where

$$\boldsymbol{\rho}^T = [\alpha \;\; \theta \;\; \chi], \;\; \boldsymbol{\ell}^T = [\ell_1 \;\; \ell_2 \;\; \ell_3 \;\; \ell_4].$$

The zero entries in the inverse Jacobian matrix indicate that the cylinder motion is independent of the corresponding joint motion. This result allows the output command for the hydraulic valve to be calculated given the desired values for $\dot{\boldsymbol{\rho}}$, since the values of $\dot{\boldsymbol{\ell}}$ are proportional to the cylinder flow rates. This aspect will be studied in more detail in Chapter 7.

Chapter 5

I/O, Sensing and Signal Conditioning

The controller relies on the information provided by the position sensor at each joint of the mechanism. The purpose of the sensors is two fold: the information is used in the kinematic calculations (the evaluation of $\mathbf{J}(\boldsymbol{\rho})$) and they provide the feedback which is used to close the feedback loop. The sensor data is filtered and the zero and span adjusted electronically before being fed into the PC. Based on this input and the operator command, the controller calculates an appropriate output which is given to the hydraulic valve. A diagram of the inputs and outputs is shown in Figure 5.1.

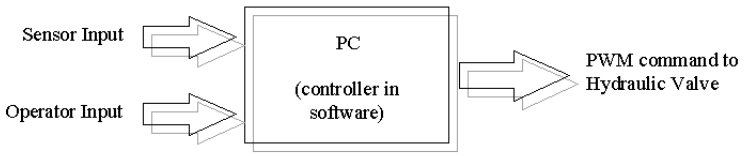

Figure 5.1: Diagram of System I/O.

5.1 Sensors

Three sensors are used to provide information about the position of the three joints. The angles of the rotational joints are measured with servo-potentiometers and the extension of the linear joint is measured with a linear displacement transducer. These type of position sensors were chosen because they provide an absolute output, which eliminates the risk of the sensor losing its position. The servo-potentiometers are conductive plastic type, with 360 degrees of mechanical rotation and 340 degrees of electrical rotation. The zero was set by adjusting their orientation in the mounting and their calibration was achieved with a spirit-level protractor to within $\pm$ 0.5 degrees. The linear displacement

transducer provides the position and velocity of the extension mast joint. The output of the sensor is 0 to 10 V d.c.. A calibrated accuracy of ± 0.5 millimeters was achieved.

5.2 The I/O Card

The interface between the PC and the real world is achieved with an electronic card housed inside the PC. This device handles the sensor inputs, the operator input and the Pulse Width Modulated (PWM) outputs. The card that was purchased for this task is an Avantech PC-LabCard; the PCL-818L. The card was selected for its performance at an affordable cost.

The I/O requirements of the system are listed in the following table:

Input/Output	Type of Signal
Sensor Inputs	Analogue, requiring conversion to digital
Operator Input	Digital, requiring at least 12 channels
PWM Output	Digital, requiring at least 12 channels

Table 5.1: I/O Requirements of Model.

The PCL-818L suffices satisfactorily. The card has 16 single-ended (or 8 differential) analogue input channels, which on cue, the card converts to 12 bit digital. It also has 16 digital input and 16 digital output channels; one 12 bit analogue output channel; and counter/timer capabilities.

5.3 Sensor Input and Signal Conditioning

The raw sensor signals are first conditioned before being supplied to the PC. As the required input voltage range of the I/O card's analogue input is ± 5 Volts, it is desirable for optimal resolution, to match the sensor input to this range. Electronic hardware was specifically designed for the task, and the gains required to do this are shown in Table 5.3. The range of the linear sensor is 0 to 10 V d.c. This has a -5V shift added to it, to match the ± 5 V I/O card input range. The rotational servo-potentiometers are mapped to ± 5 V.

Joint	Range of sensor	Range of Joint Movement	Sensor Output	Gain
α	± 170 deg	± 118 deg	± 3.47 V d.c.	1.44
θ	± 170 deg	± 31 deg	± 0.91 V d.c.	5.48
χ	± 610 mm	304 mm	± 2.46 V d.c.	2.02

Table 5.2: Sensor Signal Amplification.

The other purpose of the signal conditioning electronics was to reduce noise and to improve the noise immunity of the sensor signals. Immunity was improved by increasing

the impedance of the sensor circuit. This made the signal less susceptible to the radio frequency (RF) interference introduced in the wire between the model and the computer, and the digital noise emanating from the computer itself. Shielded wire also helped reduce the amount of RF interference.

What noise there was in the circuit was attenuated by passing the signal through a filter with a 100 Hz cut-off frequency. The filter also prevented aliasing during the analogue to digital conversion.

5.4 A/D Conversions

The sensor data was collected at 330 Hz and, with 12 bit (or 4096 count) resolution, the A/D conversion yielded the digital position with sufficient accuracy. Leaving a 20 count float at each end the joint movement divided the span into 4056 divisions. The resolution as shown in Table 5.4, is well within the calibration error:

Joint	Span of Position Sensor	A/D Resolution
α	236 degrees	0.0582 degrees per count
θ	62 degrees	0.0153 degrees per count
χ	304 mm	0.075 mm per count

Table 5.3: Digital Resolution of Joints of Model.

The sensors share a common ground and are connected to the I/O card as single-ended inputs. In hindsight, due to current loops in the ground plane of the signal conditioning circuit, it may have provided better noise immunity had the connection been differential. However, with modification and improvement to the circuit, noise levels for a static position measurement were on the order of $\pm$ 1 count.

The A/D conversions could be triggered by a number of methods. The fastest method was DMA or Direct Memory Access. Alternatively, the conversion could be software triggered, or it could be hardware triggered by internal clock or external pacer. As a high conversion rate was not required, the software trigger option was chosen.

5.5 Operator Input

The operator input was obtained by two methods. A switch box was used to input a fast, medium or slow and a forward or reverse command for each joint and fed to the PC through the I/O card's digital input channels. The second method was to use the PC's serial port, to feed a joystick command in directly.

For experimental purposes, discrete speed steps made the switch box, as shown in Figure 5.2, the most functional form of input. Its other benefit was the seamless interface with the PC. However, the most 'operator-friendly' method was the joystick. The joystick used is a six degree of freedom, computer games joystick called the SpaceOrb, as shown in Figure 5.3. As well as three translational degrees of freedom; up/down, left/right and

forward/back, the joystick has three rotational degrees of freedom; roll, pitch, and yaw. Three appropriate degrees of freedom were selected for operating the model self-loading trailer mechanism.

Figure 5.2: Switch-Box for Operator Input.

One major difficulty encountered with the joystick, was a software clash between the joystick driver and the Universal Pulse Processor (UPP) used to generate the hardware interrupt, relied upon by the controller for coordinating events. A request to the manufacturer for the joystick's source code was declined. To circumvent the problem, the I/O card's counter/timer function was utilised. This proved less effective as it relied upon catching the rising edge of the timer output flag, which was occasionally missed. The solution, however sufficed for demonstrating the SpaceOrb's capabilities.

5.6 Outputs

Given the inputs, the task of the controller is to determine the output required to drive the solenoid operated hydraulic valves, which in turn drive the hydraulic cylinders and actuate the mechanism. On the output side, the interface between the controller and the hydraulics is accomplished with the Pulsar, the solenoid operated hydraulic pilot valve. The Pulsar is designed to be operated with a digital signal, and proportional control is achieved using Pulse Width Modulation (PWM).

PWM relies on the duration that the output remains high. The state of the digital output is oscillated, being held on for a percentage of the period and off for the remainder.

Figure 5.3: *SpaceOrb* Joystick for Operator Input.

Integrated over time, the effective output is proportional to the percentage that the output is held high.

The PWM frequency is nominally 33 Hz, a value recommended by Apitech, the hydraulic valve manufacturer. Should the frequency coincide with a resonant frequency of the system, the PWM frequency can be altered. The 1/33 second period is divided into 100, giving a flow control resolution of 1%. The result of the pulses is a displacement of the flow control spool. Being forced at a far higher frequency than it can follow, the spool is shifted, allowing a hydraulic flow rate that is proportional to the PWM% value.

A second electronic circuit (see Appendix C) was designed to protect the computer from potential voltage spikes caused by the solenoid by optical isolation, and to amplify the I/O card's low powered digital output. LEDs on the output channels proved invaluable for testing and trouble shooting.

Chapter 6

Software Design

A major aspect of the project has been the design of the software. The software provides the intelligence which binds together the hardware components. The function of the software is to interpret the inputs from the sensors and from the operator, and then command the appropriate output from the hydraulic valves.

The PC was chosen as the platform for development because of the ease with which software could be designed and changes made. The programming language used is C++. C++ was chosen for its real-time speed and its flexibility.

6.1 Coordination of Events

The code is written in modular form; the main body consisting of an endless loop which idles while waiting for an interrupt. How the interrupt is generated depends on the method for obtaining the operator command. The most accurate and reliable method was to use a Universal Pulse Processor (UPP). The other method for generating the interrupt was with the PCL-818L data acquisition card's counter/timer.

The interrupt occurs at a frequency of 3300 Hz. Upon receiving the interrupt, a function which repeatedly increments a counter from 0 to 99 is called. On each count, the state of the digital outputs creating the PWM signal is checked and toggled if necessary. Other actions are also taken, depending on the value of the count. An A/D conversion occurs every tenth count(i.e. at 330 Hz). The operator input is sampled on the 91st count and the controller calculation is completed in four parts between the 95th and 98th counts. The result of the calculation is implemented 2/33rds of a second later, i.e., at the beginning of the next cycle.

6.2 PCL-818L Data Acquisition Card

The tasks of obtaining the sensor information, obtaining the operator's command, and relaying the command to the hydraulic valves, involves communication with the PCL-818L LabCard. The software driver supplied with the card proved to be too cumbersome for efficient incorporation into the controller software. Hence it was decided to write code

for controlling the card directly.

Programming the PCL-818L was relatively simple. The card uses 16 consecutive addresses in the computer's I/O space and each address corresponds to a card register. The address of each register is specified as an offset from the cards base address.

Each 8 bit register has a different function and can either be either read from or written to. For example reading from the register with the address 'Base+3' will yield the state of the first eight digital input channels (the digital input low byte). Writing to the same address with an eight bit binary number will produce an output from the first eight digital output channels. Thus the bits of the appropriate registers are manipulated to configure the PCL-818L for the desired tasks.

6.3 A/D Conversions

The analogue to digital conversions are performed following an initial setup of the PCL-818L. The initial set-up configures A/D data format, input voltage range, which channels are to be scanned, how the conversions are to be triggered, and how the data is to be transferred. The code written for the model uses a software trigger to initiate the A/D conversion and the data transfer is by program control.

Ten A/D conversions are performed per control period. The data is passed through a 4th order Butterworth digital filter with a 15 Hz cut-off frequency. The combination of the high sampling rate and the digital filtering produce results that are noise-free to sub-bit levels. The angular position can be read to one-tenth of a degree, and the linear position read to one-tenth of a millimeter.

The design of the filter can be found in Appendix D.

6.4 Post-Processing of Results

One quite major disadvantage of the software design was the difficultly in displaying and analysing information about the controller in real time. This is because printing data to the monitor interfered with the interrupt timing.

There were two solutions to this problem. The first was to use a digital oscilloscope to capture the sensor information or the PWM output. The second method proved to be more useful and consisted of saving the data to a large array, and copying the array into a file for post-analysis. The data was opened in Microsoft Excel, and a Visual Basic macro was written for quickly producing relevant graphs.

6.5 Flowchart of Software

The following figure shows the software design in diagrammatical form.

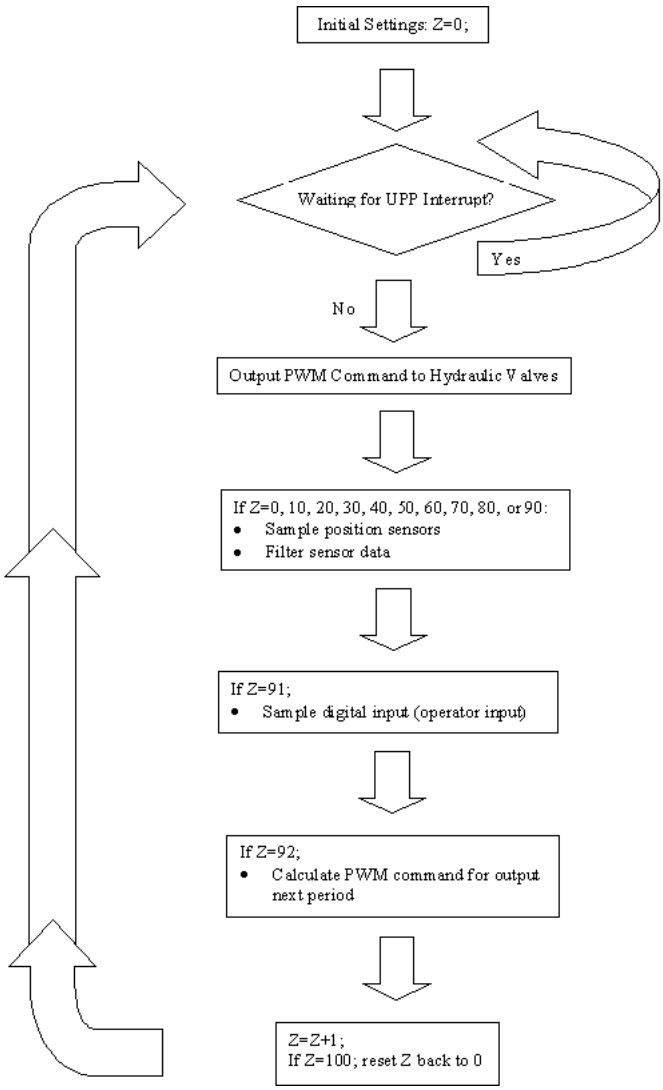

Figure 6.1: Flow Chart Outlining Software Design.

Chapter 7

Controller Design

The operator commands which direction and how fast the mechanism is to move. The final position is judged by eye. The task of the controller is to ensure that the mechanism moves in the desired fashion.

7.1 Control Strategy

Computer control of the cylinders was established once the necessary electronic hardware was constructed and the first version of software had been created. Following this achievement, position feedback was provided by mounting the linear sensor on a cylinder, thus allowing the motion and final position of an individual cylinder to be regulated.

The next level of control beyond actuating cylinders was to actuate joints. In moving joints, multiple cylinders were required to move synchronously. Control of the joints was the primary objective of the controller as once this was accomplished, joint movements themselves could be synchronised, providing the operator with the ability to command a desired movement of the payload directly, (for example a vertical motion or a horizontal motion) or the ability to make the mechanism track a path.

7.2 Velocity Feedback Controller

For actuating joints, the operator prescribes which direction and how fast the joint should move. With the switch-box input, there were three speeds; fast, medium, and slow for each joint. The joystick offered proportional control of the joint velocity. By whichever input device, the operator input signal became $\dot{\boldsymbol{\rho}}_d$, the desired joint velocities.

In the original design of controller, as shown in the block diagram of Figure 7.1, the desired joint velocity $\dot{\boldsymbol{\rho}}_d$ was compared with the actual joint velocity $\dot{\boldsymbol{\rho}}$, and the difference used to drive the system. This difference was passed through a proportional/integral (PI) controller in velocity. The controller calculates the necessary velocity to command each joint, and based on this, the Jacobian calculates the necessary velocity required from each hydraulic cylinder. The flow rate to each cylinder is related to the cylinder velocity by the cylinder's piston area, but provision must be made for the difference between

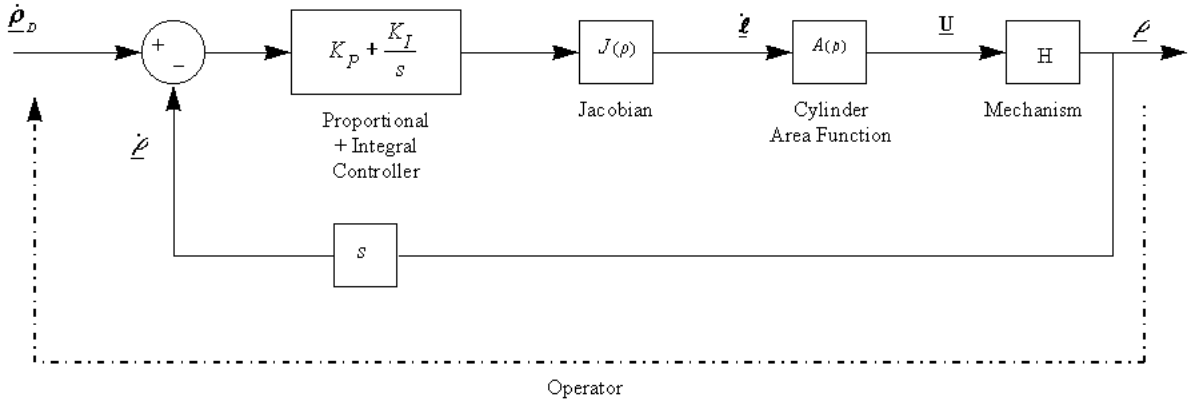

Figure 7.1: Velocity Feedback Controller.

the extension and retraction area. Cylinder velocity to flow conversion is made by the cylinder area function $\mathbf{A}(\boldsymbol{\rho})$ in the block diagram. Given the performance characteristics of the valve, the linear relationship between PWM input command $\mathbf{u}$ and output flow, $\mathbf{q}$, can be determined. This gain factor is built into the area function, $\mathbf{A}(\rho)$. The block marked $\mathbf{H}$ in the diagram represents the mechanism. As the cylinders move, the joint positions change, and the outputs are the new joint positions, $\boldsymbol{\rho}$.

The actual joint velocities were obtained by numerical differentiation of the joint positions. This is represented on the block diagram by s, the differentiation operator in the Laplace domain. Unfortunately the differentiation was the downfall of this approach to controlling the mechanism's joints. As is typical of the numerical differentiation process, the noise present in the position sensor signal was amplified, making the actual joint velocity $\dot{\boldsymbol{\rho}}$ unusable for comparison with $\dot{\boldsymbol{\rho}}_d$, the desired joint velocity.

The joint velocity is calculated by measuring the change in position over a period of time. The effect of noise on calculated velocity given a small perturbation in position data, can be understood by considering the following case. Assuming that the joint is stationary, it is quite feasible for the digitised position data to vary between samples by one bit. For the swing-arm joint, one bit amounts to 0.0582 degrees (Table 5.4). With a sampling frequency of 330 Hz, the time between samples is 1/330 seconds. Moving 0.0582 degrees in 1/330 seconds would indicate that the joint is moving at 19 degrees per second, when it is in fact stationary.

7.3 Noise Suppression Techniques

Sensor noise eminates from a number of sources. External sources such as RF interference can be minimised by passing the analogue signals through shielded cables. However this does not help reduce noise generated internally in the circuit.

The internal noise mainly came from the sensors. The greatest problem was caused by the linear transducer and the design of the signal conditioning board. The linear transducer draws bursts of current at a frequency of 2 kHz. As the power supply for the

sensors and the sensing circuitry share a common ground plane, this irregular current drain caused a voltage drop which interfered with all the sensor signals being used by the controller. Once this problem was diagnosed, the linear transducer was given a separate power supply.

The rotational sensors are servo-potentiometers, with a wiper moving over conductive plastic. Stationary readings of the rotational sensors is excellent, however when moving, the wiper tends to stick a little, creating noise.

As was described in section 5.3, noise immunity was improved by increasing the impedance of the sensor circuit. This was done by amplifying the sensor signal and helped to reduce the effects of digital noise from the connection to the computer. All of these techniques helped reduce the level of noise, but as demonstrated, the numerical differentiation process is susceptible to even low levels of noise.

In an attempt to improve the calculated joint velocities, a number of additional techniques were attempted. The sample time was increased, the position data and the calculated velocity were passed through a 4th order Butterworth digital filter. Even an analogue differentiator in electronic hardware was tried. The level of noise could be reduced, but always at the cost of introducing destabilising lag.

7.4 Velocity Feedforward, Position Feedback Controller

The question then posed was whether to purchase better quality sensors that could provide a velocity signal as well as position, or to take a new approach to controlling the joints. Consequently a new control strategy was devised: drive the system in an open-loop fashion with velocity feedforward, while ensuring tracking performance with position feedback. This strategy is presented in Figure 7.2.

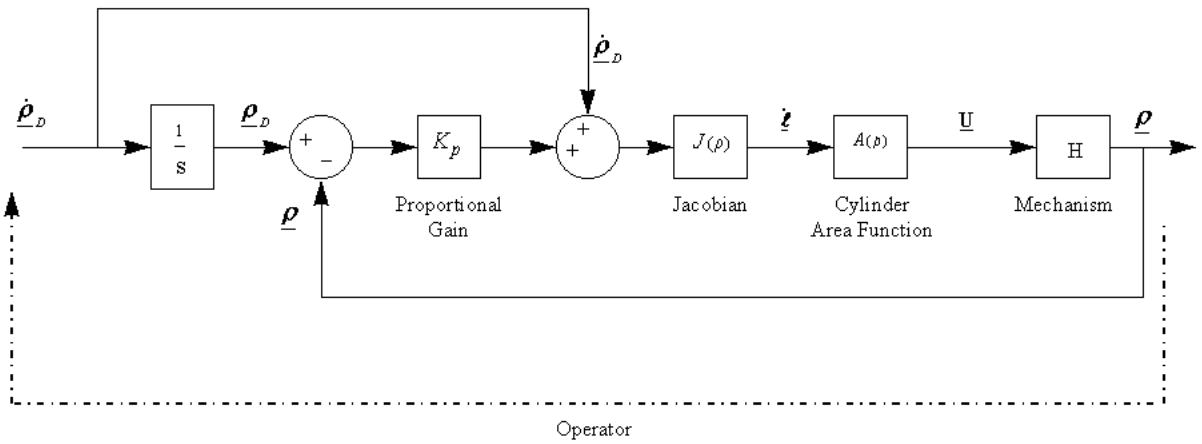

Figure 7.2: Velocity Feedforward, Position Feedback Controller.

The velocity feedforward, position feedback strategy eliminates the problems associated with numerical differentiation, as the actual joint velocity is no longer required by the controller. As with the former strategy, the operator's input is still a desired joint

velocity. This command is fed forward, and in the absence of position feedback, would drive the system open-loop. This can be understood by realising that the desired joint velocities $\dot{\boldsymbol{\rho}}_d$ are related to the desired cylinder velocities $\dot{\boldsymbol{\ell}}_d$ by:

$$\dot{\boldsymbol{\ell}}_d = \mathbf{J}(\boldsymbol{\rho})\, \dot{\boldsymbol{\rho}}_d \tag{7.1}$$

and that the desired flow rates $\mathbf{q}_d$ is related to the desired cylinder velocity $\dot{\boldsymbol{\ell}}_d$ by:

$$\mathbf{q}_d = \mathbf{A}(\boldsymbol{\rho})\, \dot{\boldsymbol{\ell}}_d \tag{7.2}$$

so that the overall relationship in the open-loop case, between the joint velocities desired by the operator, and flow to each cylinder required to produce these velocities is:

$$\mathbf{q}_d = \mathbf{A}(\boldsymbol{\rho})\, \mathbf{J}(\boldsymbol{\rho})\, \dot{\boldsymbol{\rho}}_\mathbf{d} \tag{7.3}$$

Note that $\mathbf{J}(\boldsymbol{\rho})$ is used and not $\mathbf{J}(\boldsymbol{\rho}_d)$. Using the latter would mis-map the joint-space to the ram-space as the present configuration of the mechanism would not be represented.

The open-loop system is blind and cannot correct any deviation from the desired motion that may develop. This is caused by unmodelled effects such as friction and leakage, but can be corrected with feedback. By integrating the operator's desired joint velocity to obtain desired joint position, and comparing this with the actual joint position, any deviation can be detected. Figure 7.2 shows that the error signal after the comparison of actual and desired joint positions is amplified with proportional gain and added to the velocity feedforward signal.

The velocity feedforward, position feedback strategy can be likened to the analogy that the feedforward is the d.c. gain, and the feedback is a super-imposed a.c. ripple. The feedback component is only providing fine adjustment and consequently a relatively small proportional gain $\mathbf{K}_p$ will achieve an adequate steady-state error without the need for an integral term.

7.5 Stability Proof

It is possible to show that combined feedforward/feedback renders the system globally asymptotically stable with respect to the position errors. Prior to developing this argument, consideration must be given to the fact that there are more actuators than there are degrees of freedom, in particular cylinders 1 and 2 which actuate the swing arm.

The angular position of the swing-arm joint, α can be found from the lengths of either cylinder 1 or cylinder 2. Similarly the swing-arm joint velocity can be found using the velocity of either cylinder 1 or cylinder 2:

$$\dot{\alpha} = J_{11}^{-1}(\boldsymbol{\rho})\, \dot{\ell}_1 \tag{7.4}$$

or

$$\dot{\alpha} = J_{21}^{-1}(\boldsymbol{\rho})\, \dot{\ell}_2 \tag{7.5}$$

where we have made reference to Eq. (4.9)

It should also be noted that the $J_{11}^{-1}(\boldsymbol{\rho})$ and $J_{21}^{-1}(\boldsymbol{\rho})$ do not exist at their respective cylinder's singularity. Therefore, let the information concerning the swing-arm joint, α, be determined by cylinder 1 if $\alpha > 0$, or by cylinder 2 if $\alpha \leq 0$ as defined in Figure 4.1.

Applying this rule to Eq. (4.10), either row 1 or row 2 of the matrix $\mathbf{J}(\boldsymbol{\rho})$ can be eliminated, making it square and hence invertible. Rearranging it gives

$$\dot{\boldsymbol{\rho}} = \mathbf{J}^{-1}(\boldsymbol{\rho})\, \dot{\boldsymbol{\ell}} \tag{7.6}$$

Taking the system input to be the flow rate supplied to each cylinder, let this be denoted by $\mathbf{q} = [q_{1,2} \;\; q_3 \;\; q_4]^T$ where $q_{1,2}$ denotes either valve 1 or 2 according to the above rule. The continuity equation (neglecting compressibility effects) gives $\mathbf{q} = \mathbf{A}\dot{\boldsymbol{\ell}}$ where $\mathbf{A}$ is a diagonal matrix of the appropriate cylinder areas and $\dot{\boldsymbol{\ell}}$ must be shortened appropriately. Rearranging this result, and substituting it into Eq. (7.6) yields

$$\dot{\boldsymbol{\rho}} = \mathbf{J}^{-1}(\boldsymbol{\rho})\mathbf{A}^{-1}\mathbf{q} \tag{7.7}$$

which describes the dynamics from cylinder flows to joint rates. Using Figure 7.2, the valve command is

$$\mathbf{q} = \mathbf{A}\mathbf{J}(\boldsymbol{\rho})[\dot{\boldsymbol{\rho}}_d - \mathbf{K}_p\tilde{\boldsymbol{\rho}}] \tag{7.8}$$

where $\tilde{\boldsymbol{\rho}} = \boldsymbol{\rho} - \boldsymbol{\rho}_d$ and $\mathbf{K}_p$ is a positive-definite gain matrix. Taking $V = \frac{1}{2}\tilde{\boldsymbol{\rho}}^T\tilde{\boldsymbol{\rho}}$ as a Lyapunov function for the system and using Eqs. (7.7) and (7.8),

$$\begin{aligned} \dot{V} &= \tilde{\boldsymbol{\rho}}^T[\dot{\boldsymbol{\rho}} - \dot{\boldsymbol{\rho}}_d] \\ &= \tilde{\boldsymbol{\rho}}^T[\mathbf{J}^{-1}(\boldsymbol{\rho})\mathbf{A}^{-1}\mathbf{q} - \dot{\boldsymbol{\rho}}_d] \\ &= -\tilde{\boldsymbol{\rho}}^T\mathbf{K}_p\tilde{\boldsymbol{\rho}} \end{aligned}$$

Since $\dot{V} < 0$ for $\tilde{\boldsymbol{\rho}} \neq \mathbf{0}$, the error system is globally asymptotically stable and $\tilde{\boldsymbol{\rho}} \to \mathbf{0}$ as $t \to \infty$.

7.6 Experimental Results of Control in Joint-Space

Figures 7.3 to 7.5 show the open-loop (feedforward alone, $K_p = 0$) on the left hand side, and the closed-loop tracking performance on the right, for each degree of freedom. The desired joint velocity, $\dot{\boldsymbol{\rho}}_d$, is commanded by the operator and takes the form of a constant pulse. Since the swing-arm is decoupled from the mast, its behaviour is shown in isolation (null commands were used for the mast). Figures 7.6 and 7.7 correspond to simultaneous commands for the extension and tilt joints. Note that the duration of the operator rate command is different for the open- and closed-loop cases.

In the open-loop case, the Jacobian metered out the correct rates, but a steady-state error existed owing to leakage, quantisation of the valve command, and other unmodelled effects. Increasing the proportional gain improved the rate of response and the steady-state position error, at the cost of the system becoming underdamped. Instability occurred if the gain was too high.

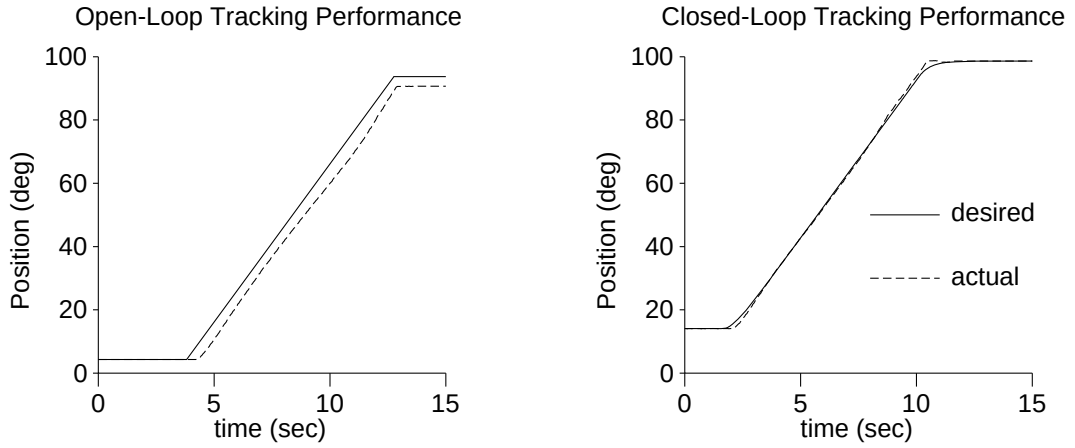

Figure 7.3: Open- and Closed-Loop Behaviour of the Swing-arm joint (α).

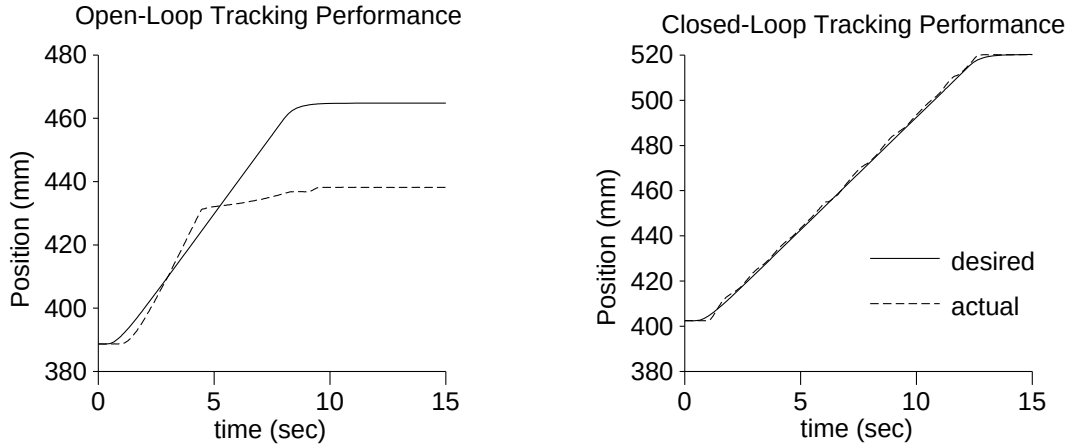

Figure 7.4: Tilt Joint (θ) with Coupled Mast Joints (θ and χ) Moved Simultaneously.

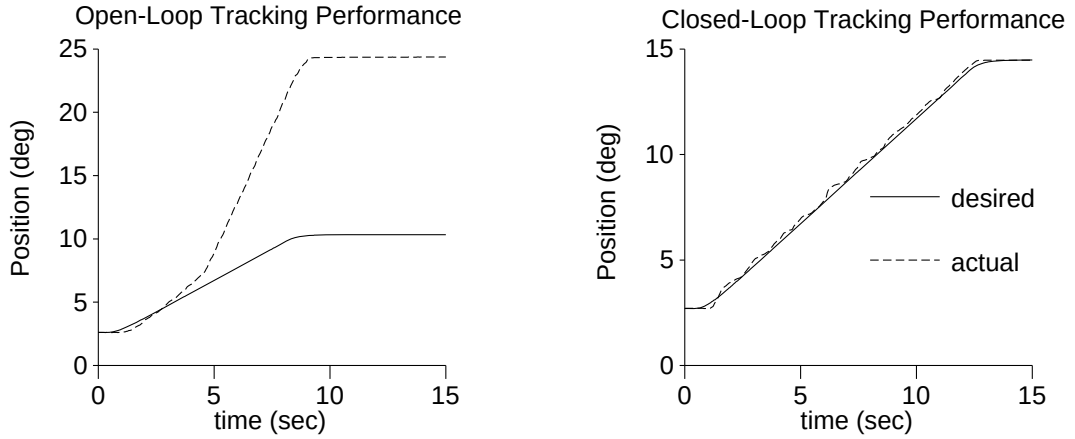

Figure 7.5: Extension Joint (χ) with Coupled Mast Joints (θ and χ) Moved Simultaneously.

$$\begin{bmatrix} 3\ sec^{-1} & 0 & 0 \\ 0 & 3\ sec^{-1} & 0 \\ 0 & 0 & 3\ sec^{-1} \end{bmatrix} \tag{7.9}$$

The proportional gains selected are shown in Eq. (7.9). The diagonal structure of the gain matrix $\mathbf{K}_p$ makes de-couples the mast and extension joint. These values of $\mathbf{K}_p$ produce the performance shown.

7.7 Task-Space Control

When moving a container, the operator would ideally like to prescribe horizontal and vertical motions, or move automatically along a pre-determined trajectory. The development of the controller has progressed from controlling individual cylinders, to controlling individual joints. The final level is to control the payload directly in the task-space.

Once control of the joints has been achieved, controlling the motion of the payload is a relatively simple one. To demonstrate the performance of the controller in task-space it was proposed to command the hook-point (where the load would be attached) to scribe a circle.

Determining the path that the joints would have to take given the circular motion of the hook-point, was done graphically. The circumference of a 400 mm diameter circle was divided into 24 segments, and the joint positions required to reach each point was measured. The alternative to doing this graphically was to find an analytical solution, which maps the task-space into the joint-space. However, for practical implementations of more general and complex paths, it was decided that the geometrical approach was more practical.

The position on the path around the circumference of the circle was regulated by a dimensionless variable, x. The value of x ranged from 0 to 24 and was used for fitting a second order interpolating polynomial between the joint positions recorded for each point. Using the difference method of interpolation, the desired joint position could be found as a function of x:

$$\boldsymbol{\rho}_d(x) = \mathbf{A}_1 + \mathbf{A}_2 x + \mathbf{A}_3 x^2 \tag{7.10}$$

where $\mathbf{A}_1, \mathbf{A}_2$, and $\mathbf{A}_3$ are vectors of coefficients calculated from the joint data of three local points.

The rate at which the circle was drawn was controlled by regulating how x evolved with time. Initially, $x = 0$ as does $\dot{x}$ and $\ddot{x}$. For a specified period of time, x increased to a specified value and a constant value of $\dot{x}$. The acceleration during this period was continuous, and finished at zero. Given these six boundary conditions for $x(t)$ and its first two derivatives, it was possible to find the six coefficients for the quintic polynomial

$$x(t) = a + bt + ct^2 + dt^3 + et^4 + ft^5 \tag{7.11}$$

After accelerating, the motion proceeded at constant velocity around the circumference of the circle, until reaching a predetermined position whereby another quintic

polynomial was found to decelerate x to a stop at the 24th point.

Differentiating Eq. (7.10) with respect to x gives

$$\frac{d\boldsymbol{\rho}_d}{dx} = \mathbf{A}_2 + 2\mathbf{A}_3 x \tag{7.12}$$

and differentiating Eq. (7.11) with respect to time, t, gives

$$\dot{x}(t) = b + 2ct + 3dt^2 + 4et^3 + 5ft^4 \tag{7.13}$$

Applying the chain rule, the desired joint velocities can be calculated:

$$\dot{\boldsymbol{\rho}}_d = \frac{d\boldsymbol{\rho}}{dx}\frac{dx}{dt} \tag{7.14}$$

With an exact solution for the velocity feedforward, $\dot{\boldsymbol{\rho}}_d$ given desired position $\boldsymbol{\rho}_d$, the approach was successful for creating a smooth interpolation of the 24 points on the circumference. The motion started from rest, accelerating smoothly to a constant speed, and then decelerated smoothly to finish at the final point.

7.8 Experimental Results of Control in Task-Space

Figure 7.6 shows the circle drawn by the mechanism. As can be seen, there is some deviation from desired path, but the general shape is obvious. Figures 7.7 to 7.9 show the desired and actual joint paths that are required to create the circular motion of the hook-point. Note that the extension joint is required to remain at a constant value throughout the movement, and it does so to within 2 mm despite the path taken by the coupled tilt joint. The path tracking error is mainly due to finite resolution of control over the flow rate. Note the flat, stationary points in Figures 7.7 and 7.8 when the joint changes direction. This is a symptom of the dead band in the spool. In this region of the graph, the commanded flow-rates are less than what is delivered by the smallest increment of the controller output, 1 % PWM. The result is bang-bang' type control.

Nevertheless, the performance is well acceptable for the task of loading containers.

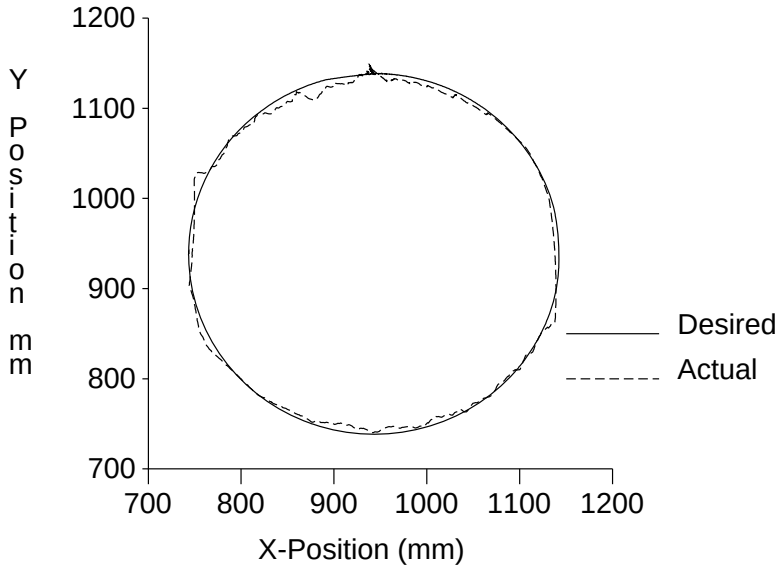

Figure 7.6: Path Traced by Hook-Point.

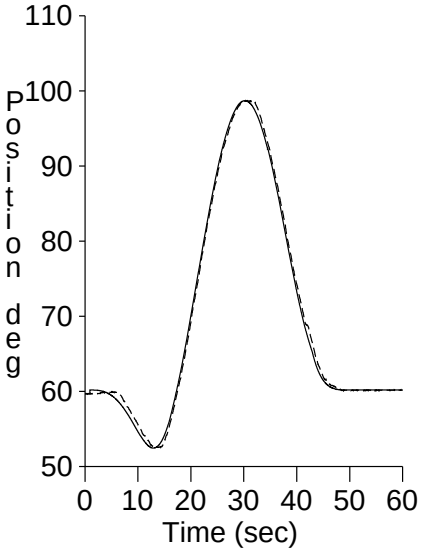

Figure 7.7: Path Traced by Swing-Arm Joint (α).

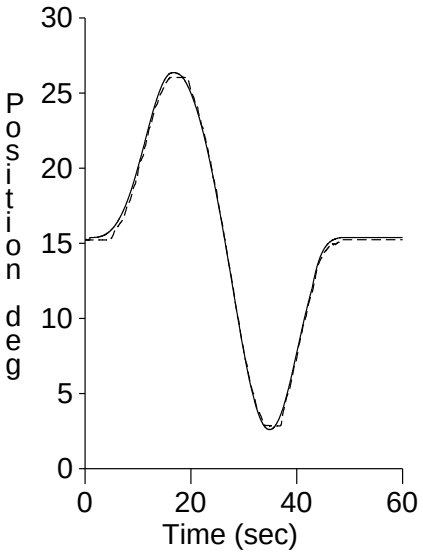

Figure 7.8: Path Traced by Tilt Joint (θ).

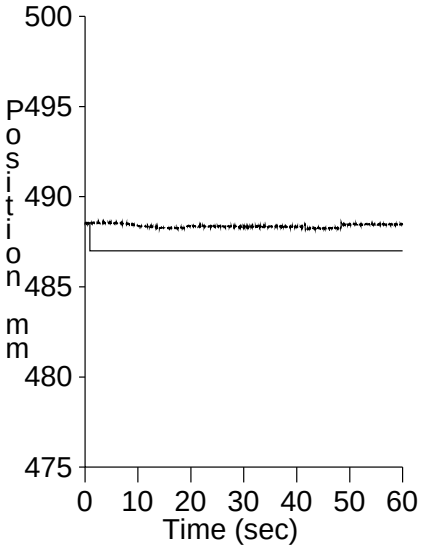

Figure 7.9: Path Traced by Extension Joint (χ).

Chapter 8

Conclusion

8.1 Achievement of Master's Study

The aim of the Master's study was to design, build and control a half-scale working model of the proposed mechanism in order to determine whether the concept of the design could be realised. This objective has been achieved, and the development has revealed no unsurmountable problem with the concept, from a control perspective.

The combined feedforward/feedback control strategy chosen, is shown to provide excellent tracking performance. This form of controller will be employed in the full-sized mechanism.

8.2 Realisation of Full-Sized Prototype

The working model has been very beneficial in the development of the dual-sided self-loading trailer. It has facilitated the design of many aspects of the system: the hydraulic circuit, the sensing, signal conditioning and I/O, the software and the controller itself. All this has been achieved with minimal financial risk to the companies involved.

The project focus is beginning to shift towards development of the full-sized version. The adaptation of the controller to suit the real application has begun, the purchase of solid modelling software for the detailed mechanical design is planned, and discussion is underway with a potential manufacturer. Since the GRIF contract expired at the end of September 1997, the student has been employed by A.M.E.S., and is continuing to work full-time on the project.

All parties involved in the project can see the potential of the design for filling the niche in the market. Thus the project will continue with the aim of having a full-sized prototype built by mid-1998.

Bibliography

[**1**] *Road and Traffic Standards Information*, Land Transport Safety Authority of New Zealand, No. 2, Revision 1, August 1994, pp. 1.

[**2**] *Road and Traffic Standards Information*, Land Transport Safety Authority of New Zealand, No. 2, Revision 1, August 1994, pp. 7.

[**3**] Merritt, Herbert E., *Hydraulic Control Systems*, pp. 76-84, New York: Wiley, 1967.

[**4**] Anderson, Wayne R.., *Controlling Electrohydraulic Systems*, New York: Dekker, 1988.

[**5**] Hunt T. & Vaughan N., *Hydraulic Handbook*, Oxford: Elsevier Science Ltd., 1996.

[**6**] Yealpe, Frank., *Fluid Power Design Handbook*, New York: Dekker, 1996.

[**7**] Shigley J.E., *Mechanical Engineering Design*, McGraw-Hill Book Company, 1986.

[**8**] Stefani R.T. et al.., *Design of Feedback Control Systems*, Saunders College Publishing, 1992.

Appendix A

Workshop Drawings of Model

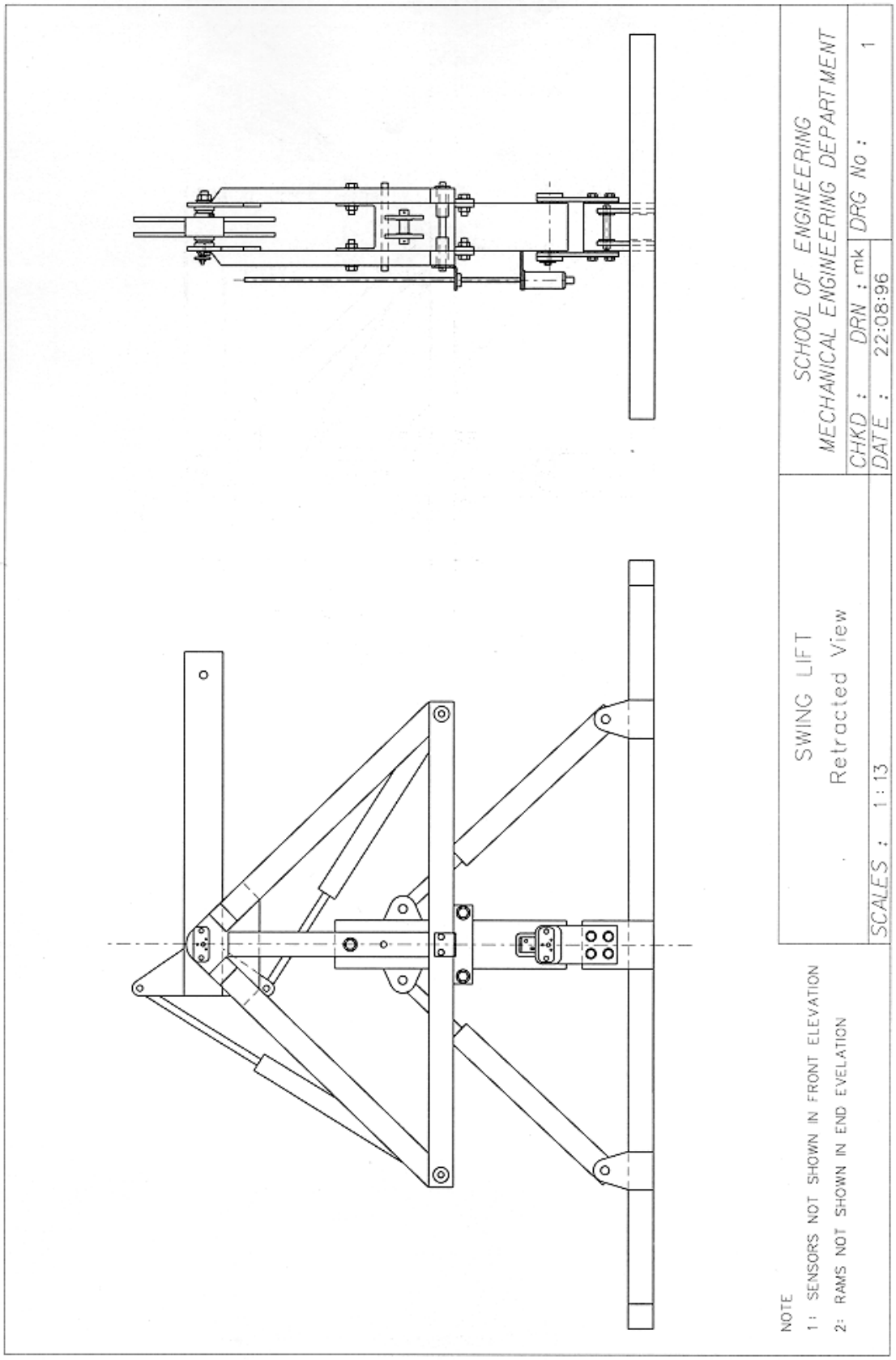
SCHOOL OF ENGINEERING
MECHANICAL ENGINEERING DEPARTMENT
CHKD :
DRN : mk
DRG No : 1
DATE : 22:08:96
SCALES : 1:13
SWING LIFT
Retracted View
NOTE
1: SENSORS NOT SHOWN IN FRONT ELEVATION
2: RAMS NOT SHOWN IN END EVELATION

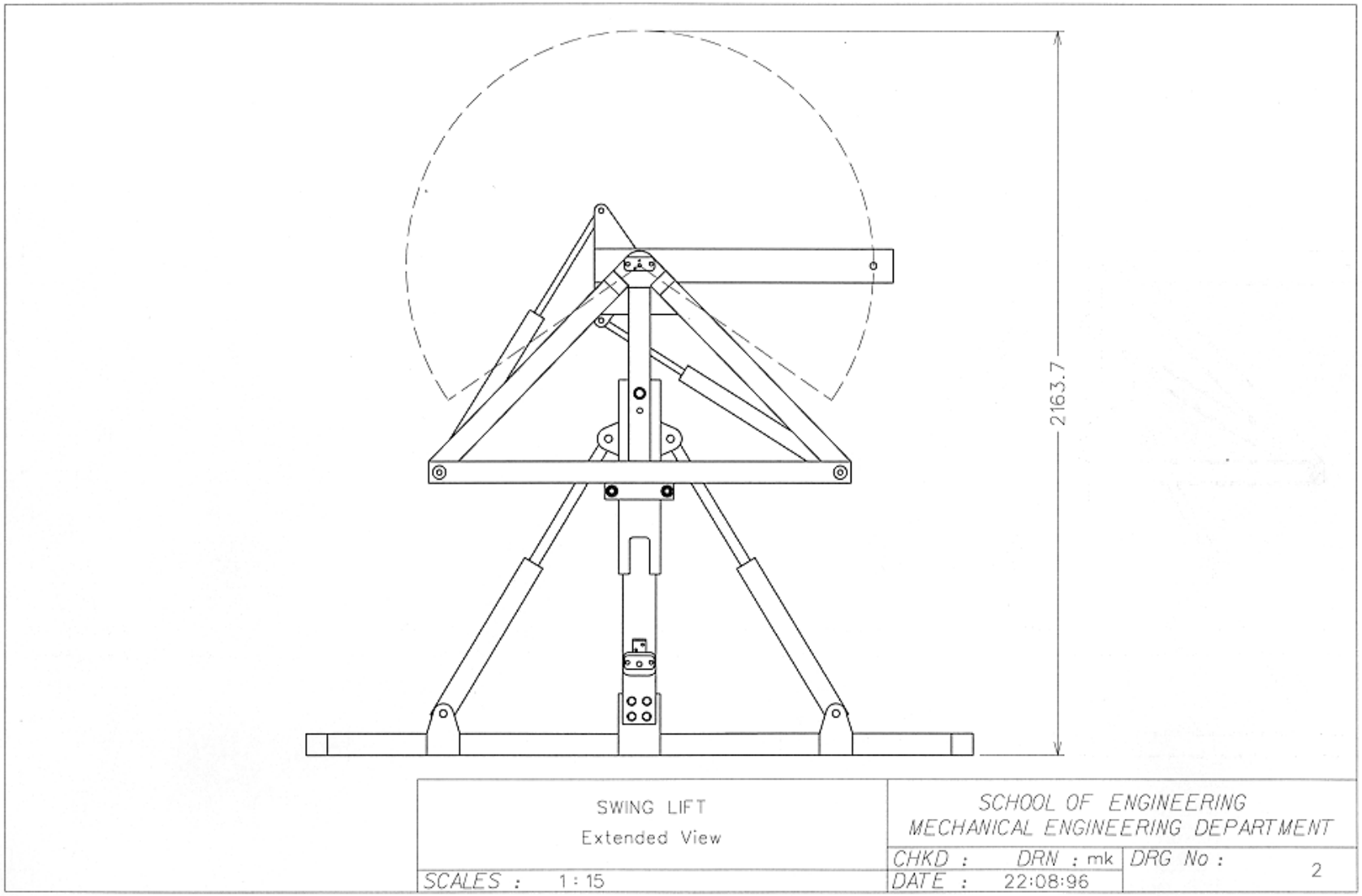
2163.7
SWING LIFT
Extended View
SCALES : 1 : 15
SCHOOL OF ENGINEERING
MECHANICAL ENGINEERING DEPARTMENT
CHKD : DRN : mk
DATE : 22:08:96
DRG No : 2

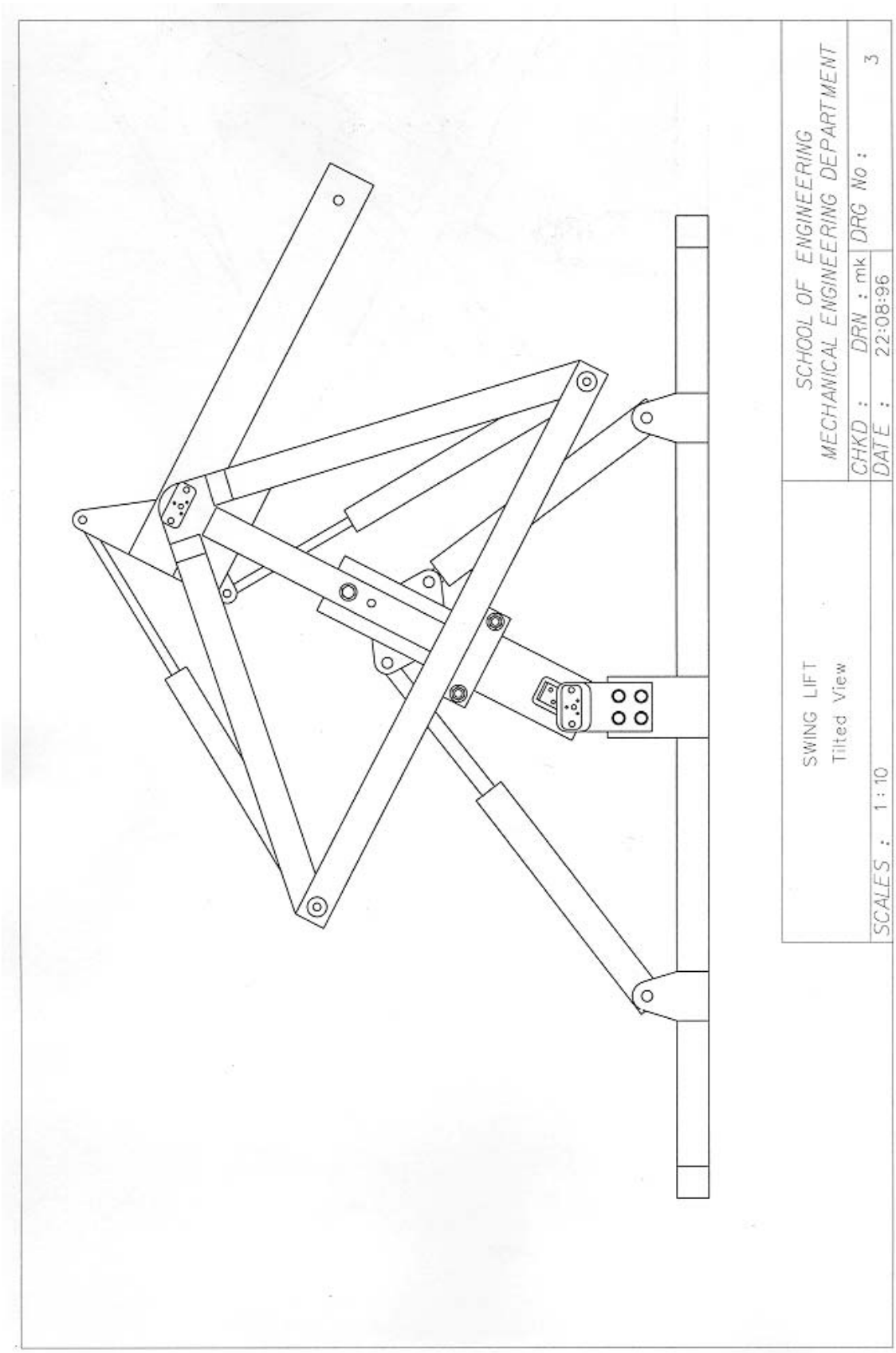
SCHOOL OF ENGINEERING
MECHANICAL ENGINEERING DEPARTMENT
SWING LIFT
Tilted View
SCALES : 1:10
CHKD :
DRN : mk
DRG No : 3
DATE : 22:08:96

VIEW WITH FRONT A-FRAME
REMOVED AND MAST IN SECTION

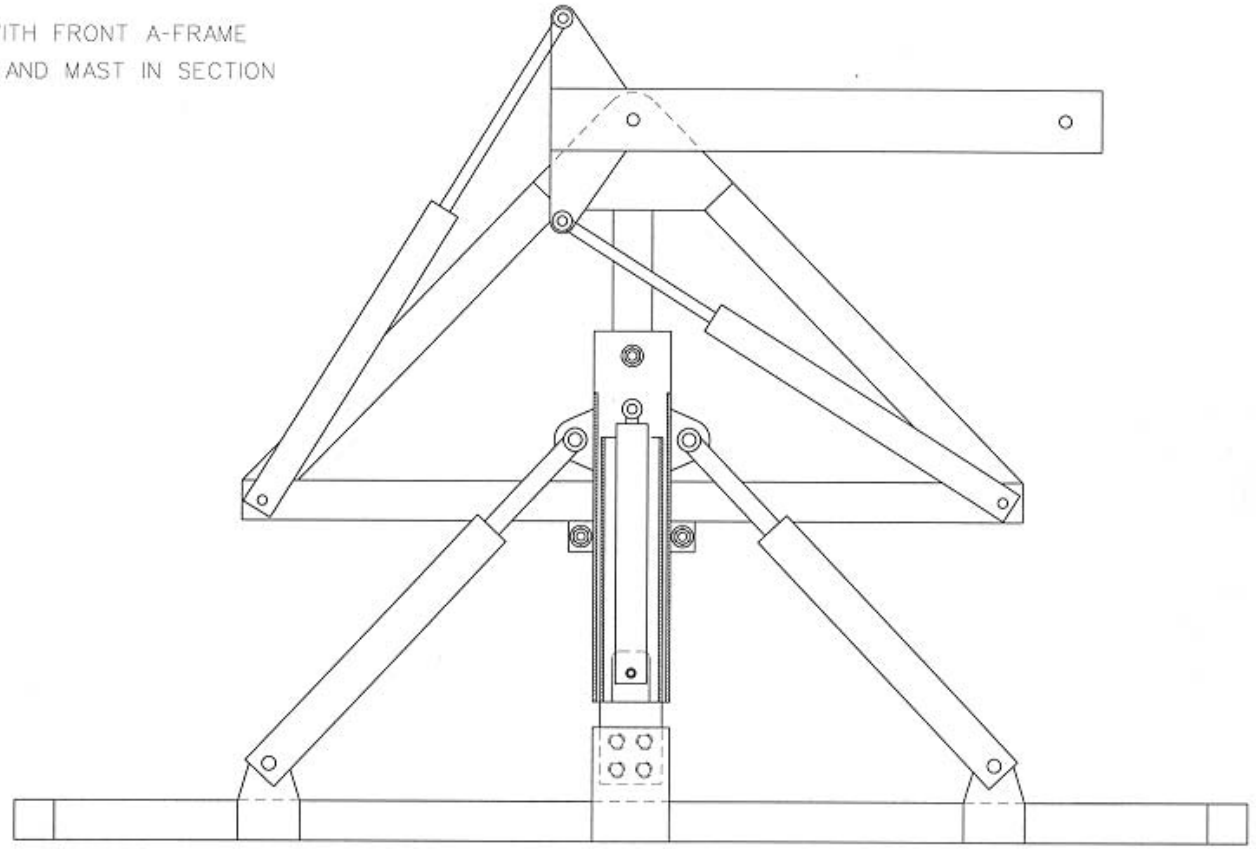

SWING LIFT Front Section	SCHOOL OF ENGINEERING MECHANICAL ENGINEERING DEPARTMENT
SCALES : 1 : 10	CHKD : DRN : mk DATE : 22:08:96
	DRG No : 4

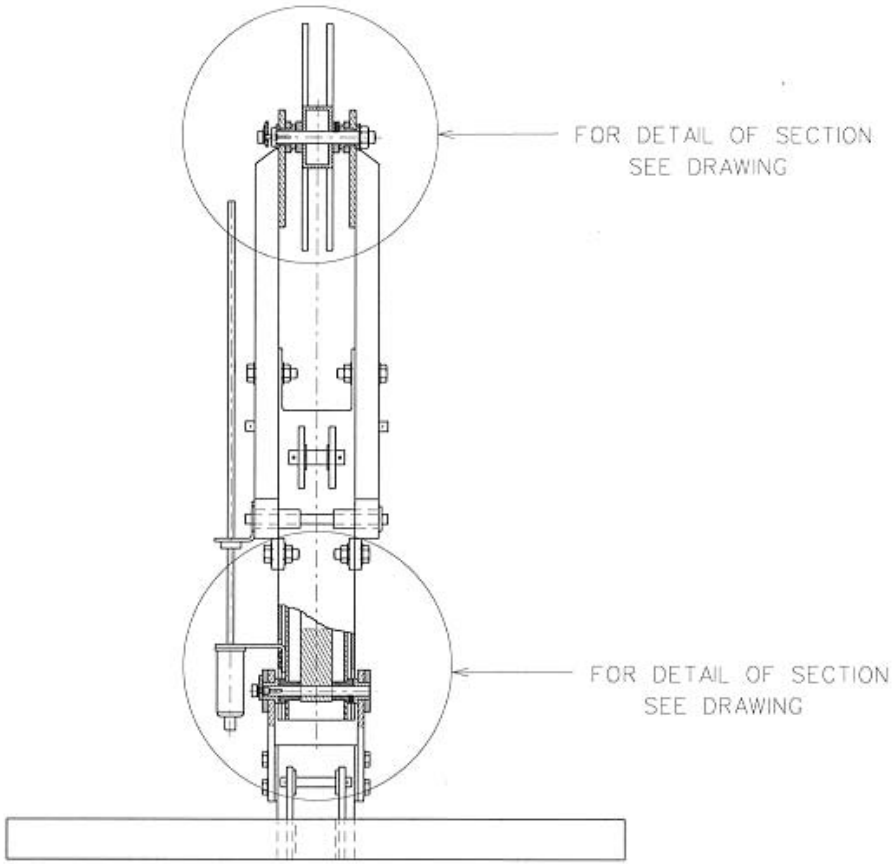

SWING LIFT Detailed Section	SCHOOL OF ENGINEERING MECHANICAL ENGINEERING DEPARTMENT
SCALES : 1:10	CHKD : DRN : mk DATE : 22:08:96
	DRG No : 5

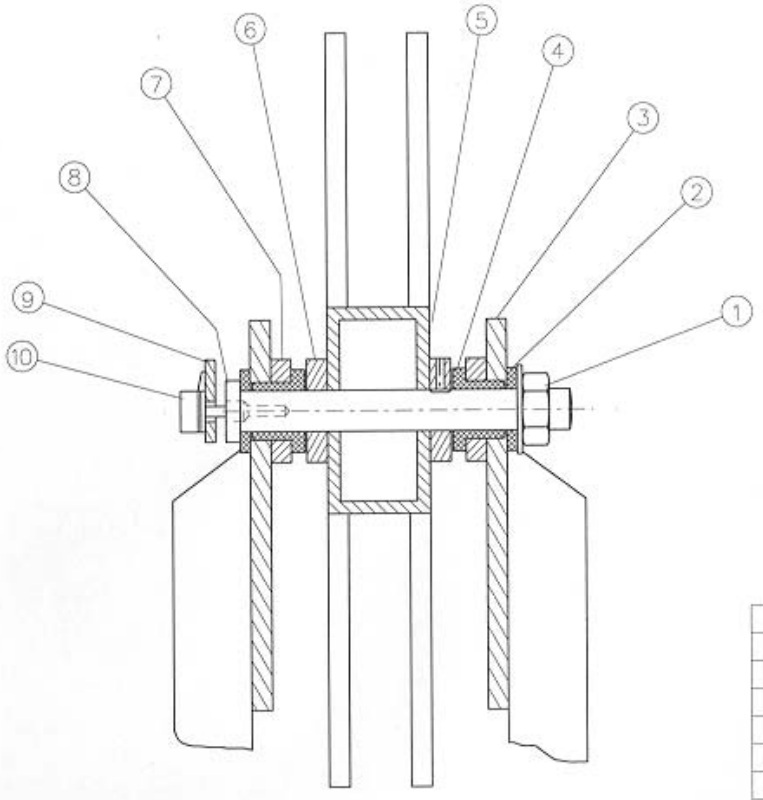

ITEM	DESCRIPTION	QUANTITY
10	Rotational Sensor	1
9	Sensor Mount Plate	1
8	Swing Arm Pivot Pin (shoulder)	1
7	Bearing Block	2
6	Spacer Block	2
5	Swing Arm	1
4	Plastic Bush	2
3	Top Plate	2
2	Plastic Washer	2
1	Nut, M20	1

SWING LIFT
Section 2

SCALES : 1:3

SCHOOL OF ENGINEERING
MECHANICAL ENGINEERING DEPARTMENT

CHKD : DRN : mk

DATE : 22:08:96

DRG No : 6

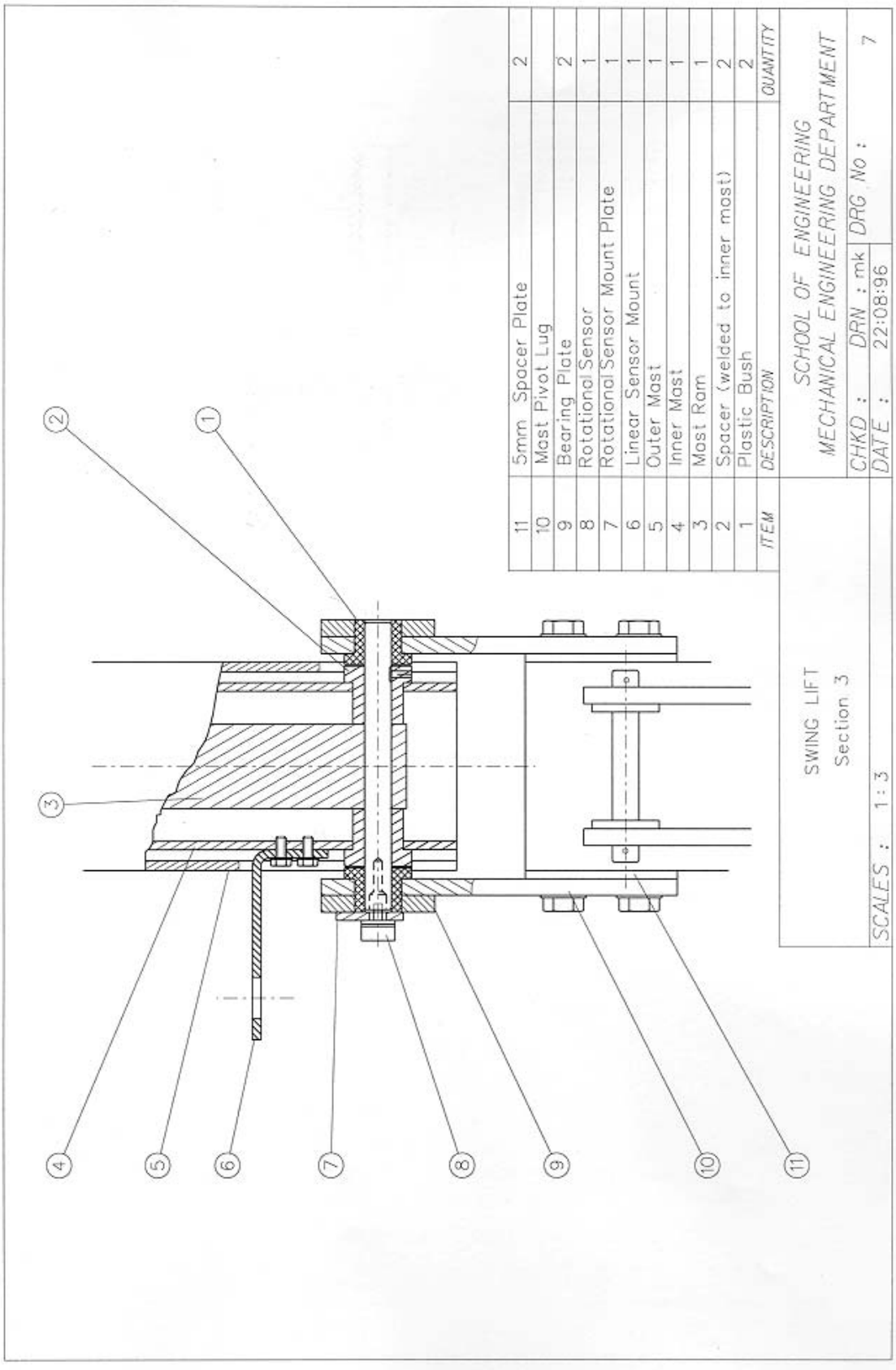
SCHOOL OF ENGINEERING
MECHANICAL ENGINEERING DEPARTMENT
SWING LIFT
Section 3
SCALES : 1:3
CHKD :
DRN : mk
DATE : 22:08:96
DRG No : 7
ITEM | DESCRIPTION | QUANTITY
11 | 5mm Spacer Plate | 2
10 | Mast Pivot Lug |
9 | Bearing Plate | 2
8 | Rotational Sensor | 1
7 | Rotational Sensor Mount Plate | 1
6 | Linear Sensor Mount | 1
5 | Outer Mast | 1
4 | Inner Mast | 1
3 | Mast Ram | 1
2 | Spacer (welded to inner mast) | 2
1 | Plastic Bush | 2

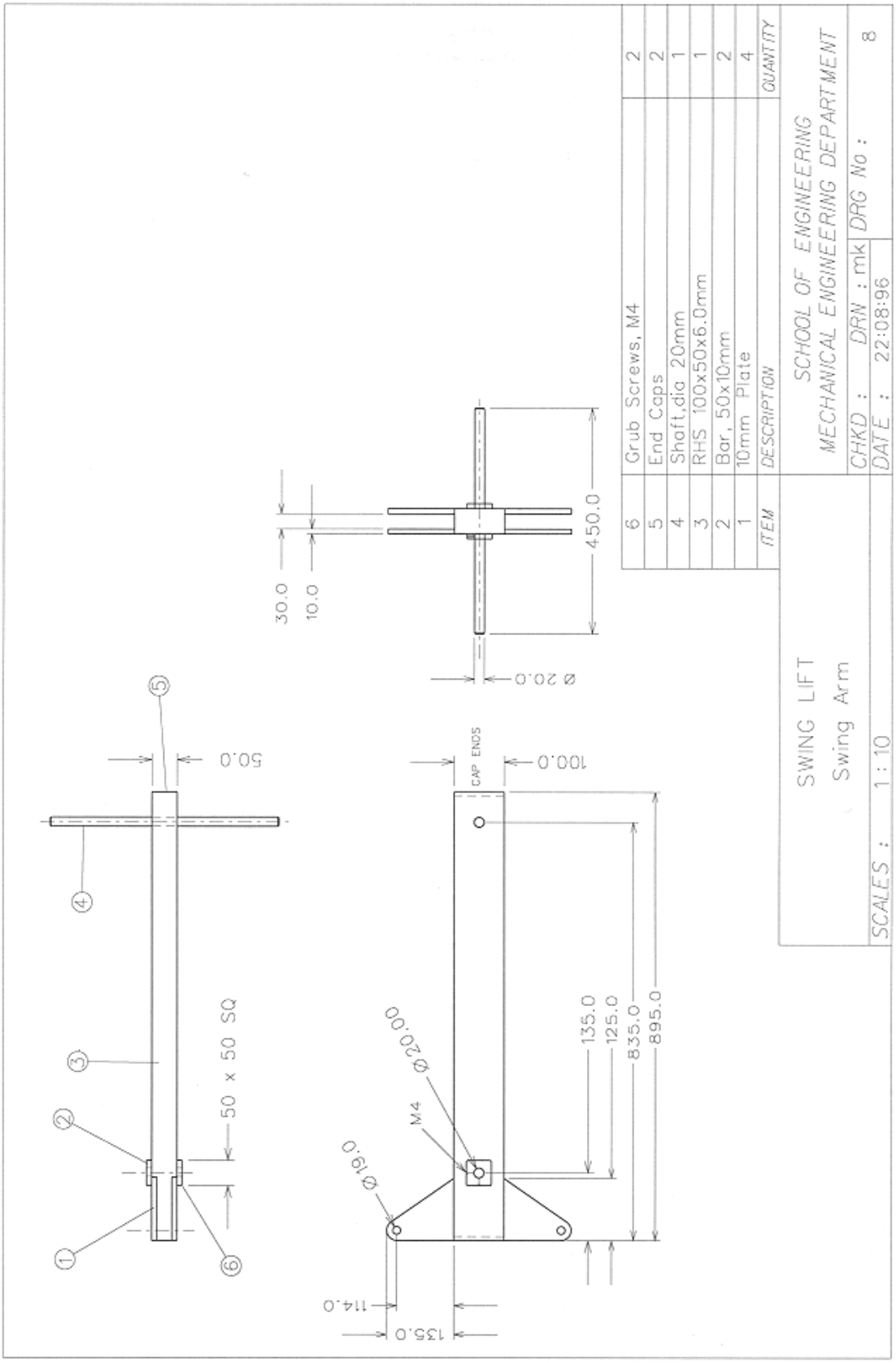
SWING LIFT
Swing Arm
SCHOOL OF ENGINEERING
MECHANICAL ENGINEERING DEPARTMENT
SCALES : 1:10
CHKD :
DRN : mk
DATE : 22:08:96
DRG No : 8
ITEM
DESCRIPTION
QUANTITY
6 Grub Screws, M4 2
5 End Caps 2
4 Shaft,dia 20mm 1
3 RHS 100x50x6.0mm 1
2 Bar, 50x10mm 2
1 10mm Plate 4
450.0
30.0
10.0
Ø 20.0
50.0
100.0
CAP ENDS
50 x 50 SQ
135.0
125.0
835.0
895.0
Ø20.00
M4
Ø19.0
114.0
135.0

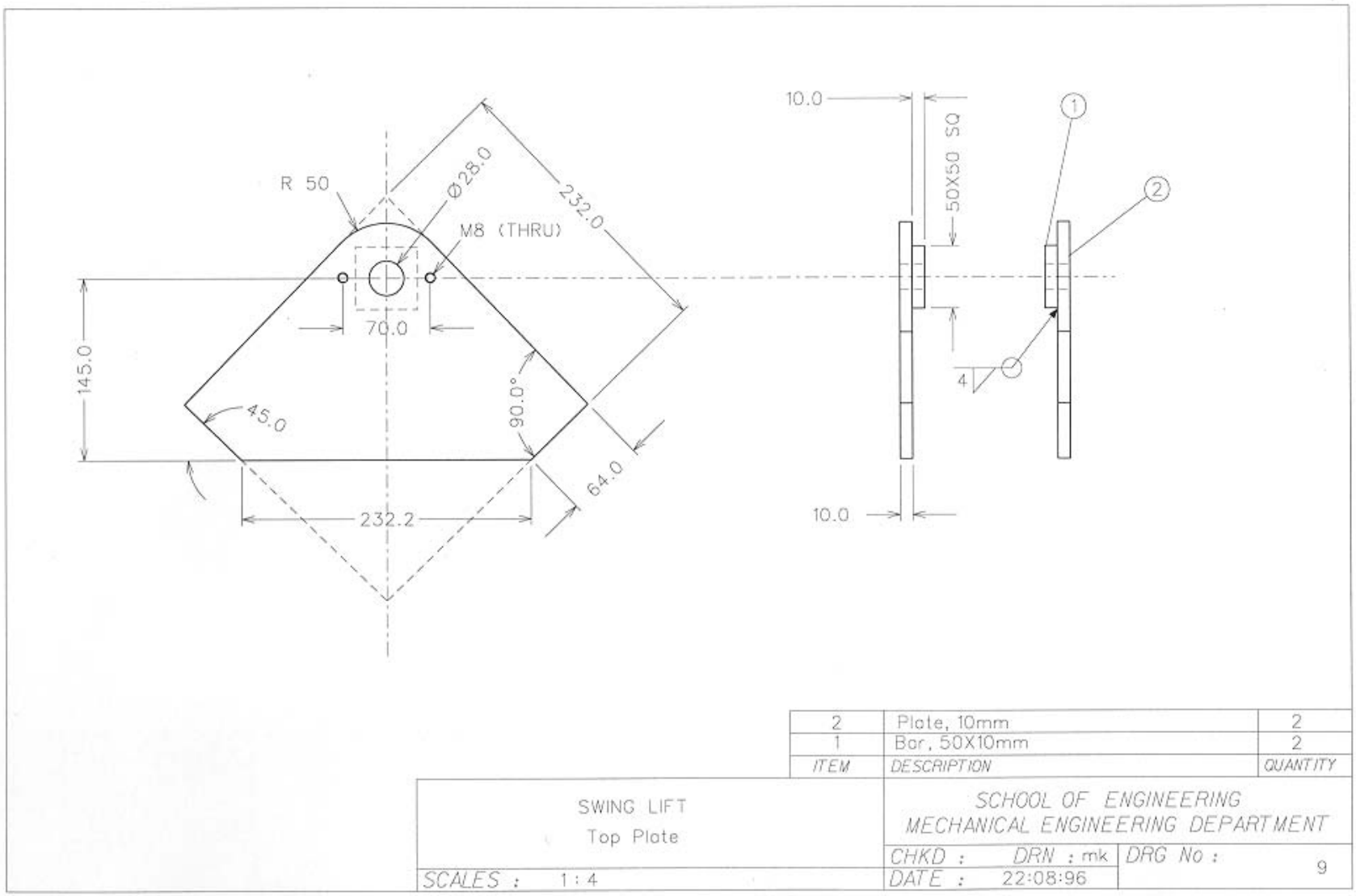

ITEM	DESCRIPTION	QUANTITY
2	Plate, 10mm	2
1	Bar, 50X10mm	2

SWING LIFT
Top Plate

SCHOOL OF ENGINEERING
MECHANICAL ENGINEERING DEPARTMENT

CHKD : DRN : mk DRG No : 9

SCALES : 1 : 4 DATE : 22:08:96

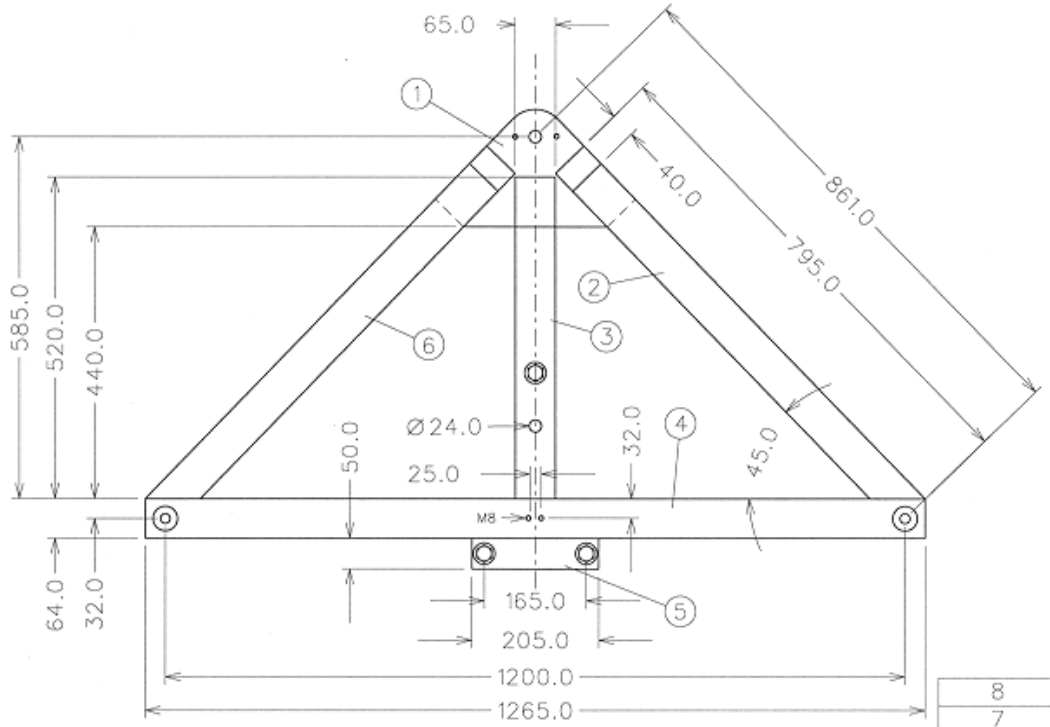

ITEM	DESCRIPTION	QUANTITY
8	MS bar (see dwg 20)	2
7	M16 Bolt	6
6	RHS, 64x83x4.0mm	2
5	Bar, 50x10mm	2
4	RHS, 64x83x4.0mm	2
3	RHS, 64x83x4.0mm	2
2	RHS, 64x83x4.0mm	2
1	Top Plate (see dwg 9)	2

SWING LIFT
A-Frame

SCALES : 1 : 10

SCHOOL OF ENGINEERING
MECHANICAL ENGINEERING DEPARTMENT

CHKD : DRN : mk

DATE : 22:08:96

DRG No : 10

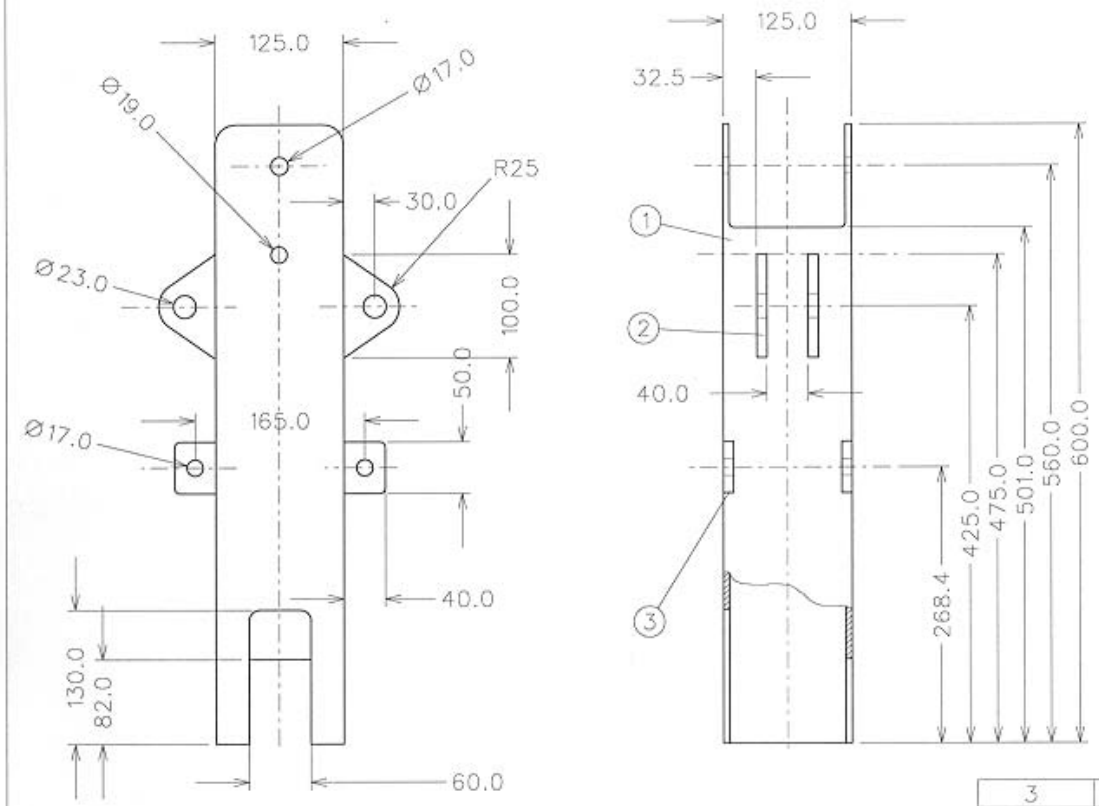

ITEM	DESCRIPTION	QUANTITY
3	A-Frame Lug, Flat Bar, 50x10mm	4
2	Side Ram Lug, Plate 100x10mm	4
1	Square RHS, 125x125x6.0mm	1

SWING LIFT
Mast Outer

SCHOOL OF ENGINEERING
MECHANICAL ENGINEERING DEPARTMENT

CHKD : DRN : mk DRG No : 11

SCALES : 1 : 6 DATE : 22:08:96

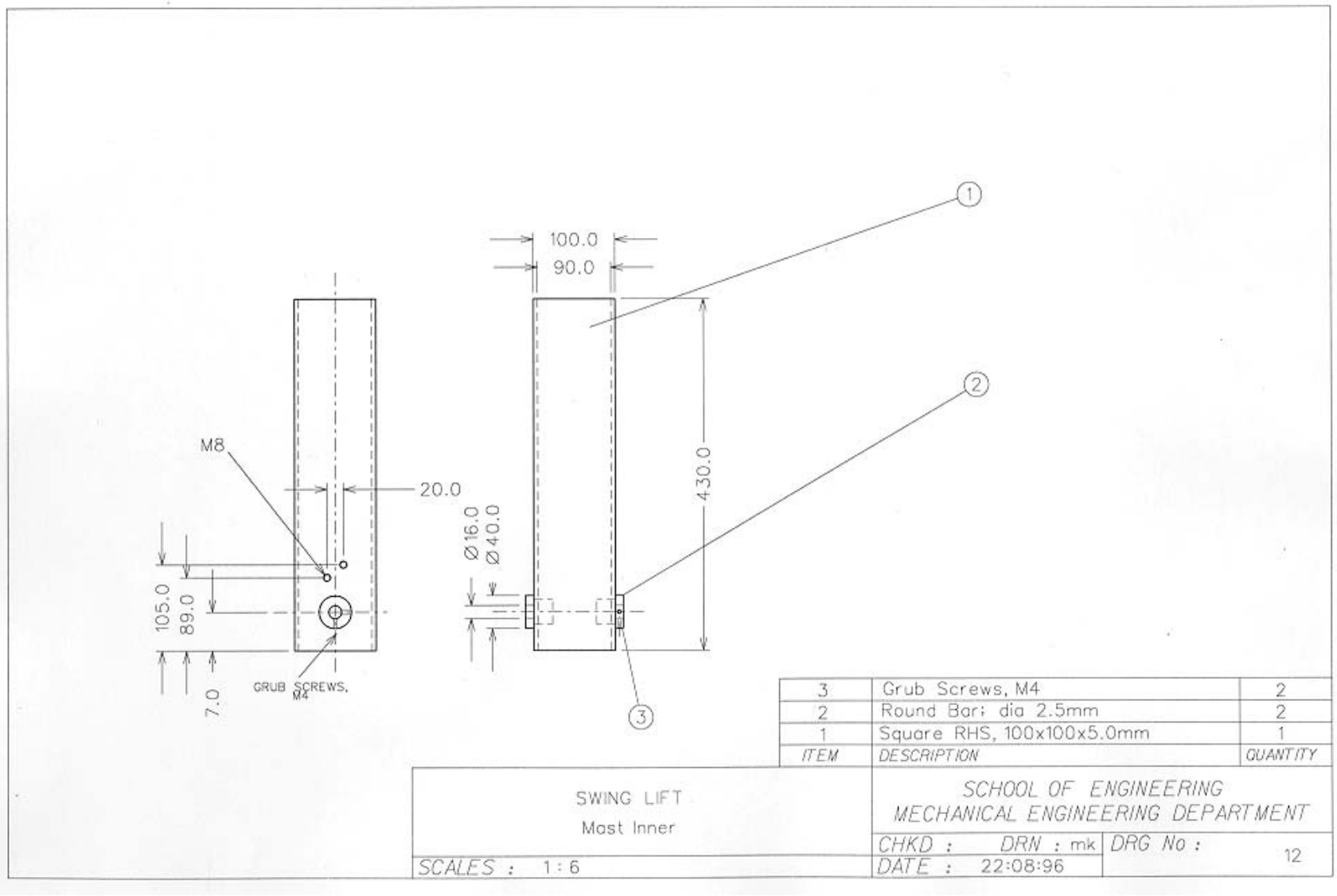

ITEM	DESCRIPTION	QUANTITY
3	Grub Screws, M4	2
2	Round Bar; dia 2.5mm	2
1	Square RHS, 100x100x5.0mm	1

SWING LIFT
Mast Inner

SCALES : 1 : 6

SCHOOL OF ENGINEERING
MECHANICAL ENGINEERING DEPARTMENT

CHKD : DRN : mk

DATE : 22:08:96

DRG No : 12

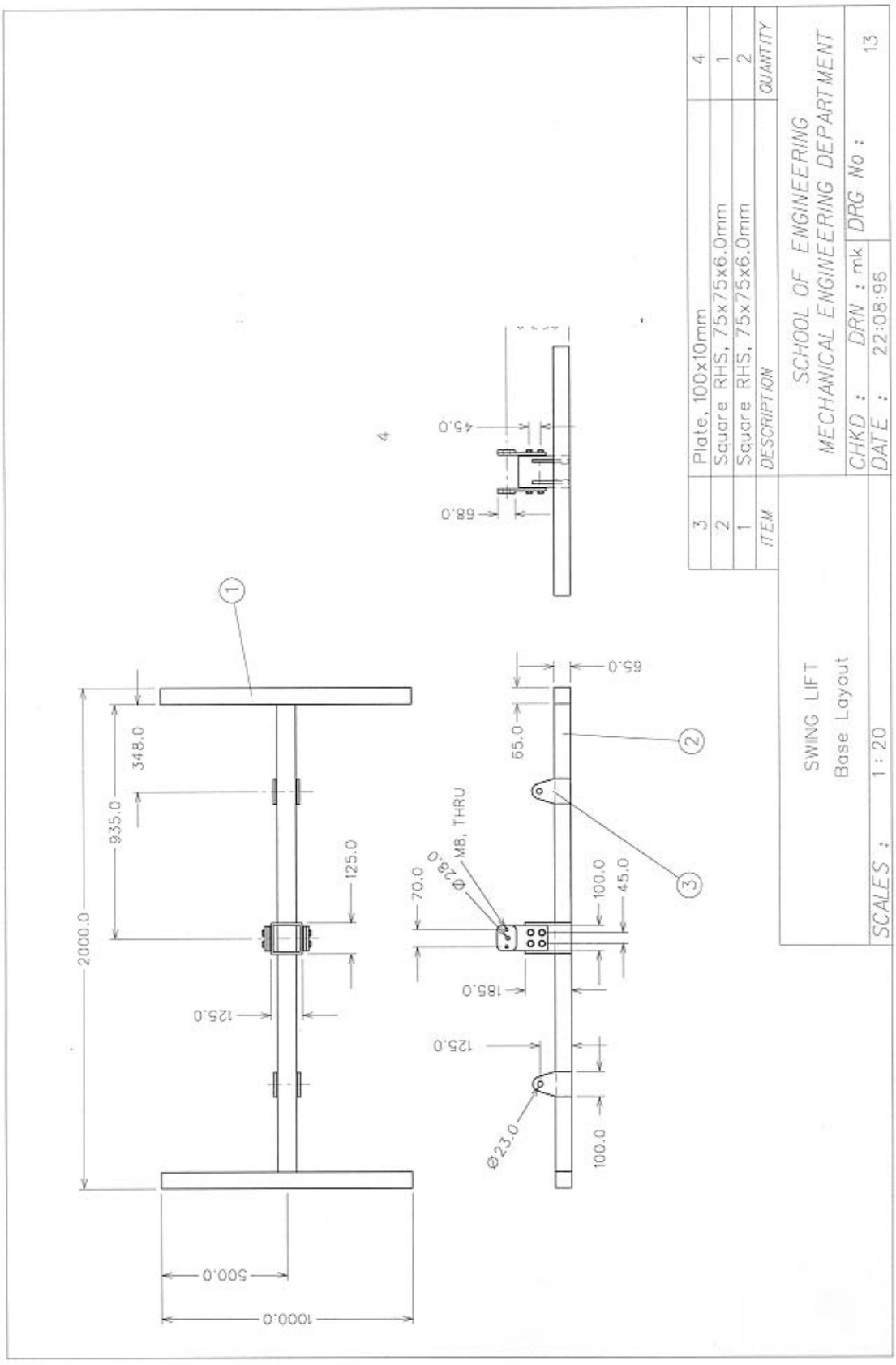
4
45.0
68.0
1
348.0
935.0
125.0
2000.0
125.0
500.0
1000.0
65.0
65.0
2
3
70.0
Φ8.0
M8, THRU
100.0
45.0
185.0
125.0
Ø23.0
100.0
3 Plate, 100x10mm 4
2 Square RHS, 75x75x6.0mm 1
1 Square RHS, 75x75x6.0mm 2
ITEM DESCRIPTION QUANTITY
SCHOOL OF ENGINEERING
MECHANICAL ENGINEERING DEPARTMENT
SWING LIFT
Base Layout
SCALES : 1:20
CHKD : DRW : mk DRG No : 13
DATE : 22:08:96

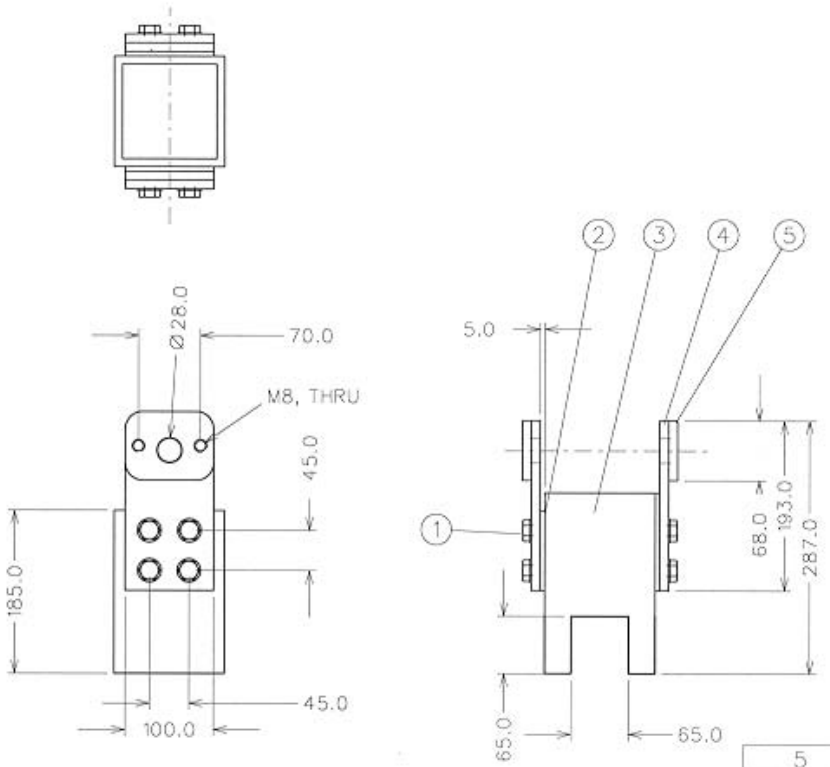

ITEM	DESCRIPTION	QUANTITY
5	Bearing Plate, Flat Bar, 50x10mm	2
4	Ram Lug, Plate, 100x10mm	2
3	Square RHS, 125x125x9.0mm	1
2	Spacer Plate, 100x75x5mm	2
1	Bolts, M112 x 30mm	8

SWING LIFT
Mast Base

SCALES : 1 : 7

SCHOOL OF ENGINEERING
MECHANICAL ENGINEERING DEPARTMENT

CHKD : DRN : mk

DATE : 28:08:96

DRG No : 14

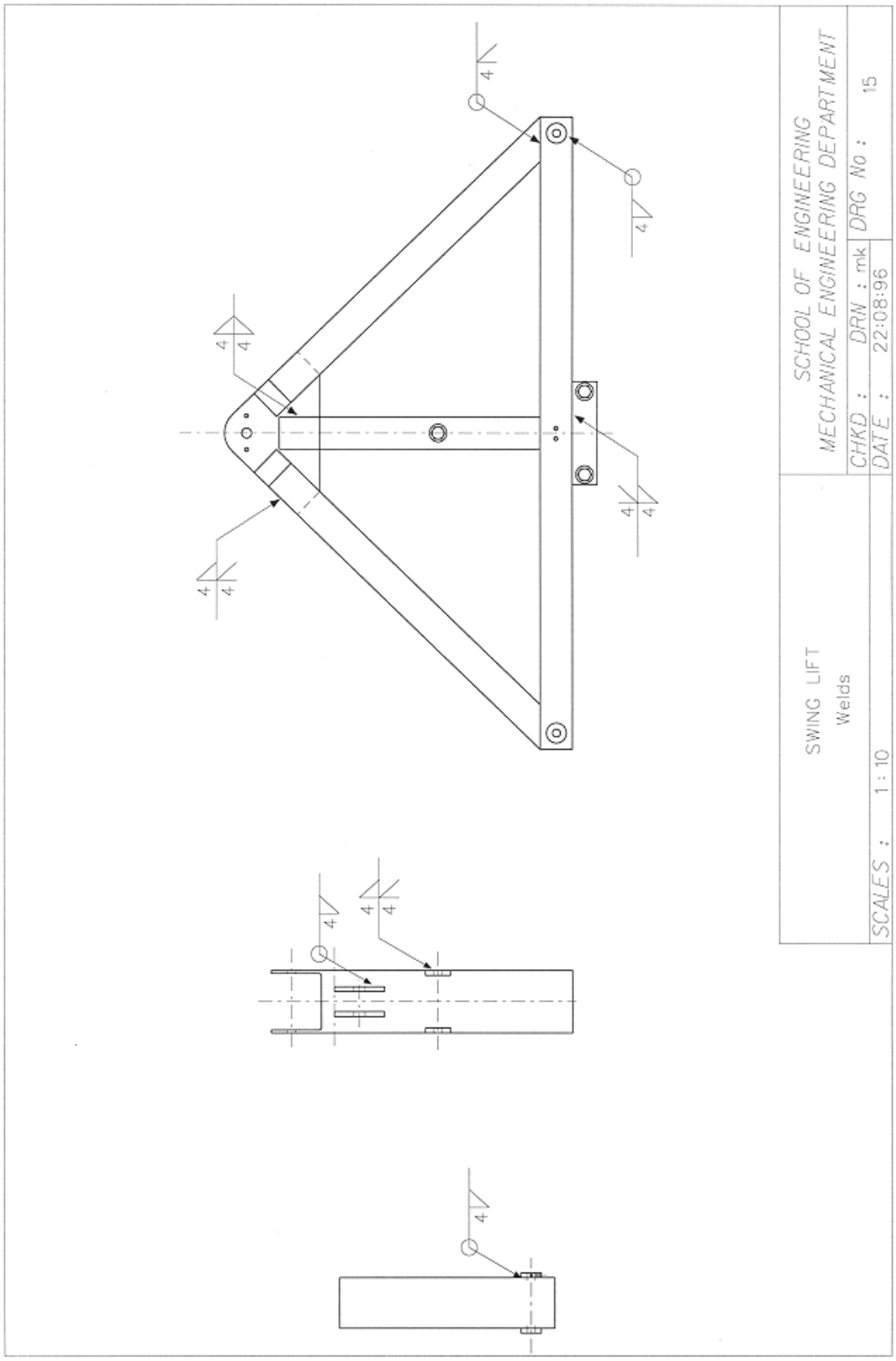
SCHOOL OF ENGINEERING
MECHANICAL ENGINEERING DEPARTMENT
CHKD : DRW : mk DRG No : 15
DATE : 22:08:96
SWING LIFT
Welds
SCALES : 1 : 10
4

4
4
4
4
4
4
4
4
4
4
4
SWINGLIFT
Welds
SCALES : 1:10
SCHOOL OF ENGINEERING
MECHANICAL ENGINEERING DEPARTMENT
CHKD : DRN : mk
DATE : 22:08:96
DRG No : 16

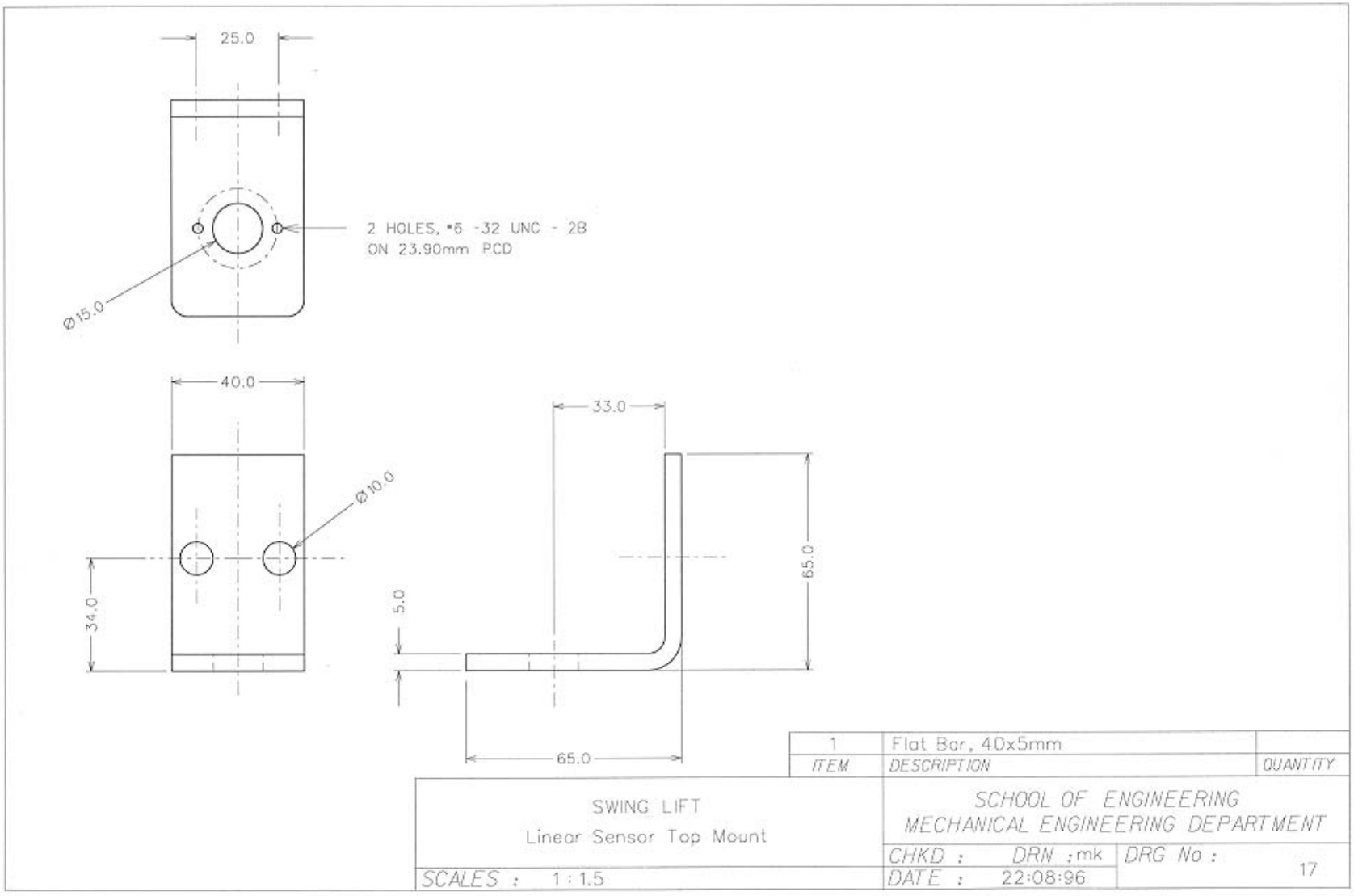

ITEM	DESCRIPTION	QUANTITY
1	Flat Bar, 40x5mm	

SWING LIFT
Linear Sensor Top Mount

SCHOOL OF ENGINEERING
MECHANICAL ENGINEERING DEPARTMENT

CHKD : DRN : mk DRG No : 17

SCALES : 1 : 1.5 DATE : 22:08:96

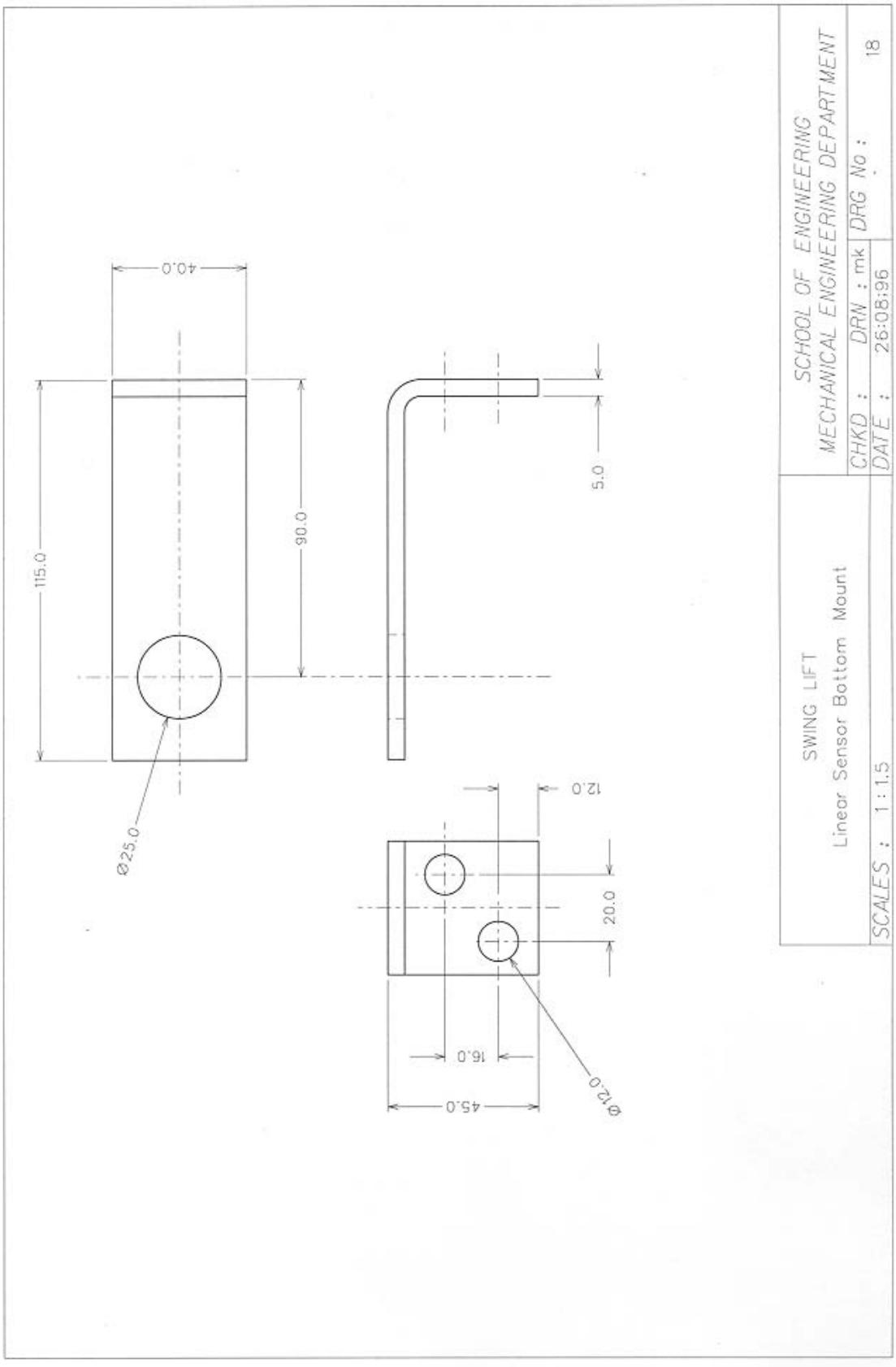
40.0
115.0
90.0
5.0
Ø25.0
12.0
20.0
16.0
45.0
Ø12.0
SCHOOL OF ENGINEERING
MECHANICAL ENGINEERING DEPARTMENT
CHKD :
DRW : mk
DRG No : 18
DATE : 26:08:96
SWING LIFT
Linear Sensor Bottom Mount
SCALES : 1:1.5

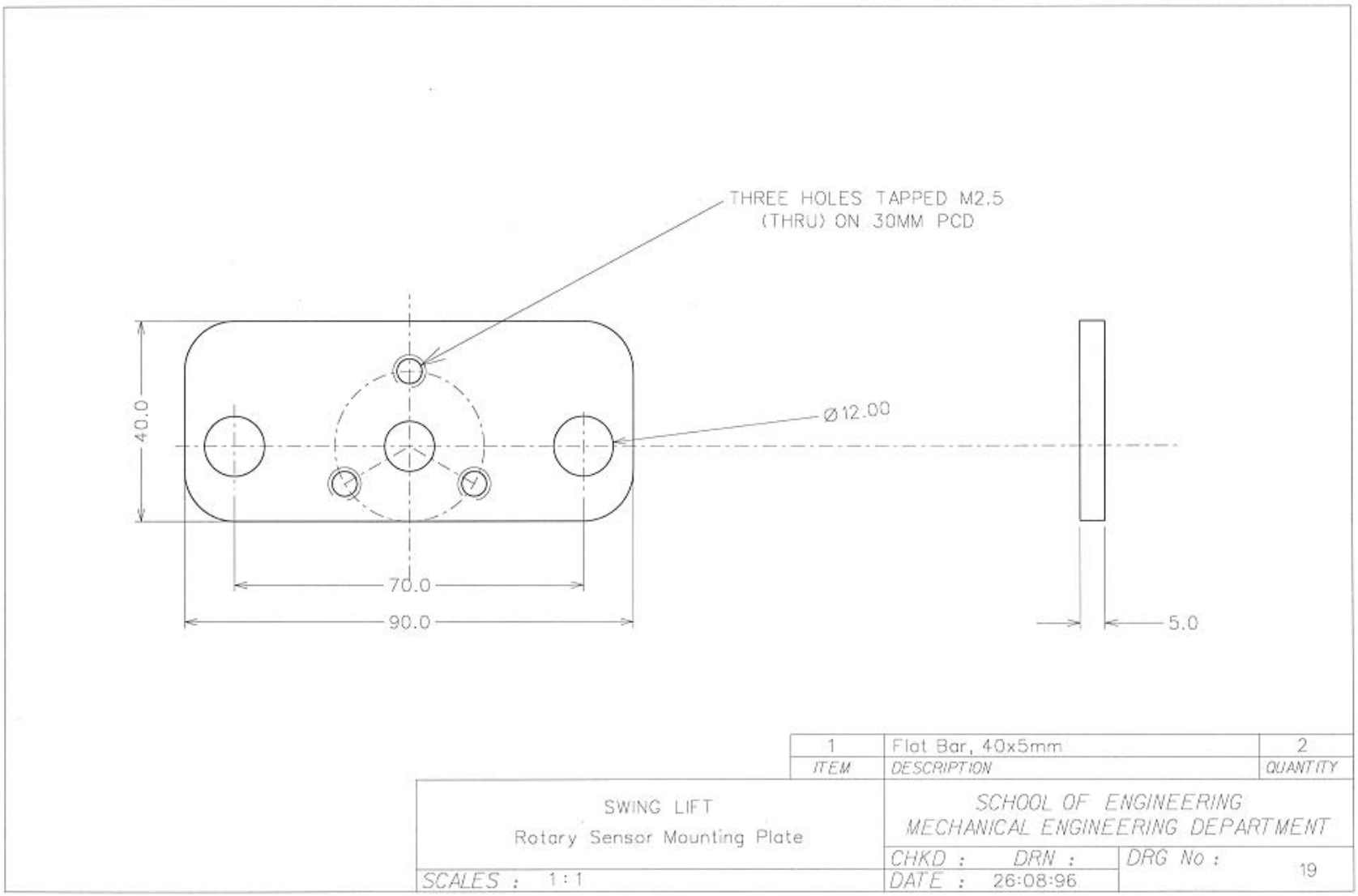

ITEM	DESCRIPTION	QUANTITY
1	Flat Bar, 40x5mm	2

SWING LIFT Rotary Sensor Mounting Plate	SCHOOL OF ENGINEERING MECHANICAL ENGINEERING DEPARTMENT	
SCALES : 1:1	CHKD : DRN : DATE : 26:08:96	DRG No : 19

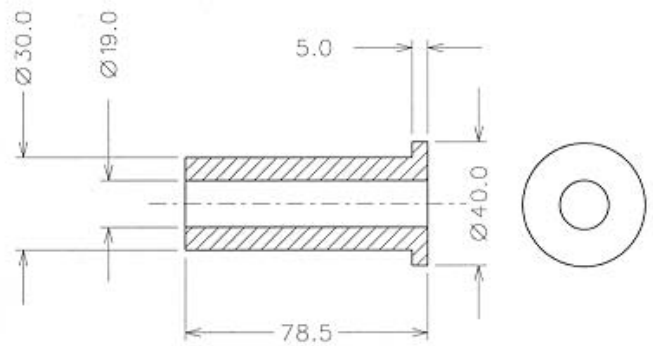

A-FRAME BOSS

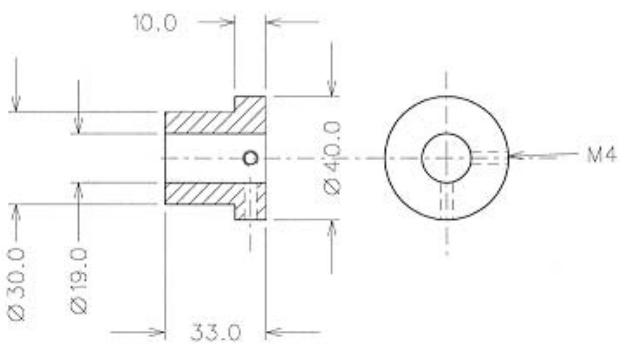

BEARING BOSS

ITEM	DESCRIPTION	QUANTITY
2	Inner Mast Bearing Boss (MS Bar)	2
1	A-Frame Bosses (MS Bar)	4

SWING LIFT
Bosses

SCALES : 1 : 2

SCHOOL OF ENGINEERING
MECHANICAL ENGINEERING DEPARTMENT

CHKD : DRN : mk

DATE : 26:08:96

DRG No : 20

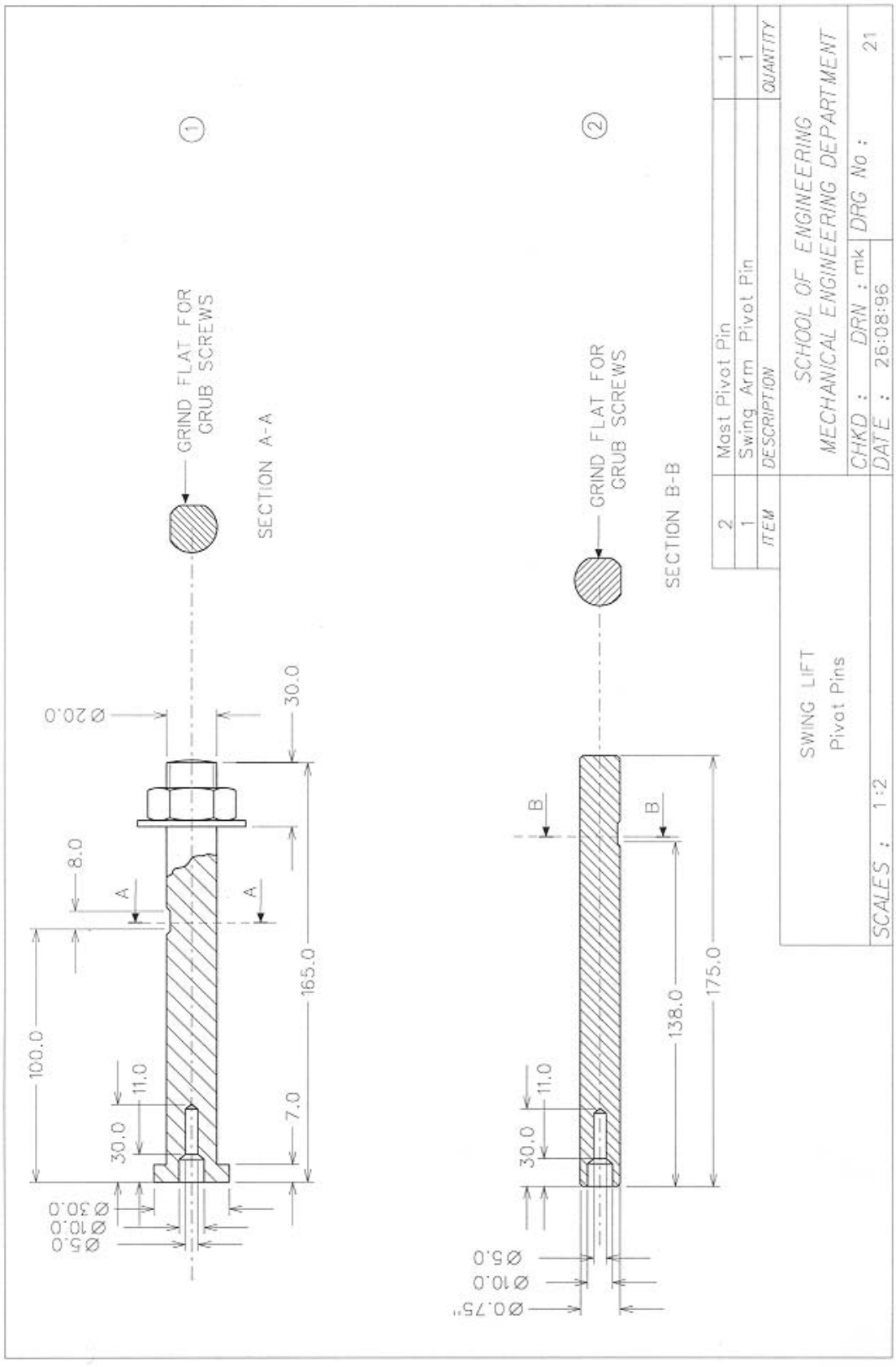
GRIND FLAT FOR GRUB SCREWS
SECTION A-A
SECTION B-B
Ø20.0
30.0
8.0
A
100.0
11.0
30.0
165.0
7.0
Ø30.0
Ø10.0
Ø5.0
B
138.0
175.0
Ø0.75"
2 Mast Pivot Pin 1
1 Swing Arm Pivot Pin 1
ITEM DESCRIPTION QUANTITY
SCHOOL OF ENGINEERING
MECHANICAL ENGINEERING DEPARTMENT
SWING LIFT
Pivot Pins
SCALES : 1:2
CHKD : DRN : mk DRG No : 21
DATE : 26:08:96

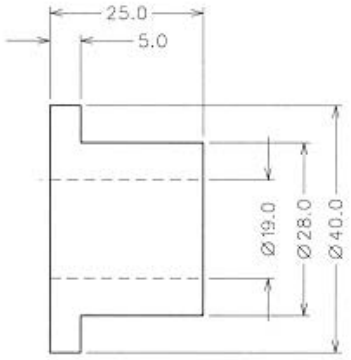

① MAST PIVOT

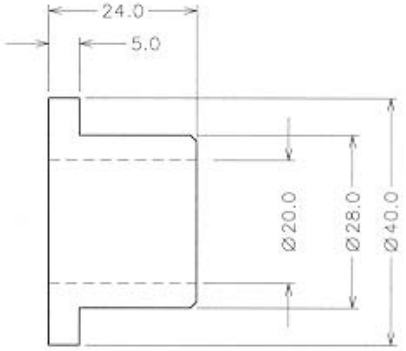

② SWING ARM PIVOT

ITEM	DESCRIPTION	QUANTITY
2	Swing Arm Pivot Bearing (PETP)	2
1	Mast Pivot Bearing (PETP)	2

SWING LIFT
Plastic Bearings

SCALES : 1:2

SCHOOL OF ENGINEERING
MECHANICAL ENGINEERING DEPARTMENT

CHKD : DRN : mk

DATE : 26:08:96

DRG No : 22

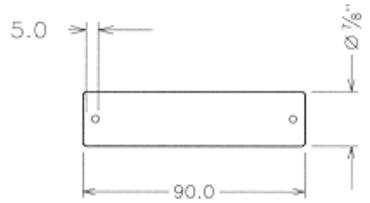

(1) Mast Side Ram Top Pin

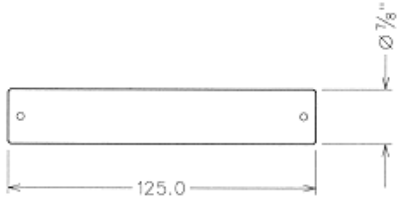

(2) Mast Side Ram Bottom Pin

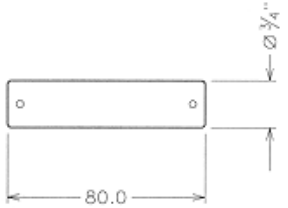

(3) Swing Arm Ram Top Pin

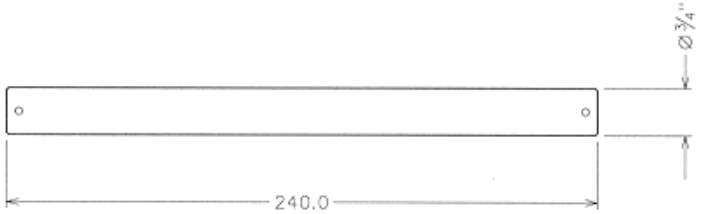

(4) Swing arm Ram Bottom Pin

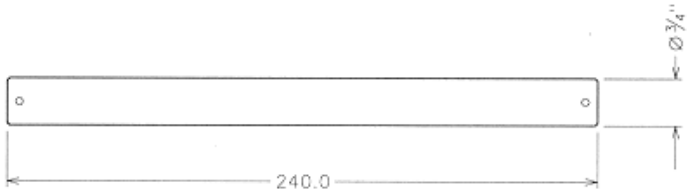

(5) Mast Centre Ram Top Pin

ITEM	DESCRIPTION	QUANTITY
5	Bright Free Cutting Bar; dia 3/4"	1
4	Bright Free Cutting Bar; dia 3/4"	2
3	Bright Free Cutting Bar; dia 3/4"	2
2	Bright Free Cutting Bar; dia 7/8"	2
1	Bright Free Cutting Bar; dia 7/8"	2

SWING LIFT
Ram Pins

SCHOOL OF ENGINEERING
MECHANICAL ENGINEERING DEPARTMENT

CHKD : DRN : mk
DRG No : 23
SCALES : 1 : 2.5
DATE : 26:08:96

Appendix B

Hydraulic Circuit

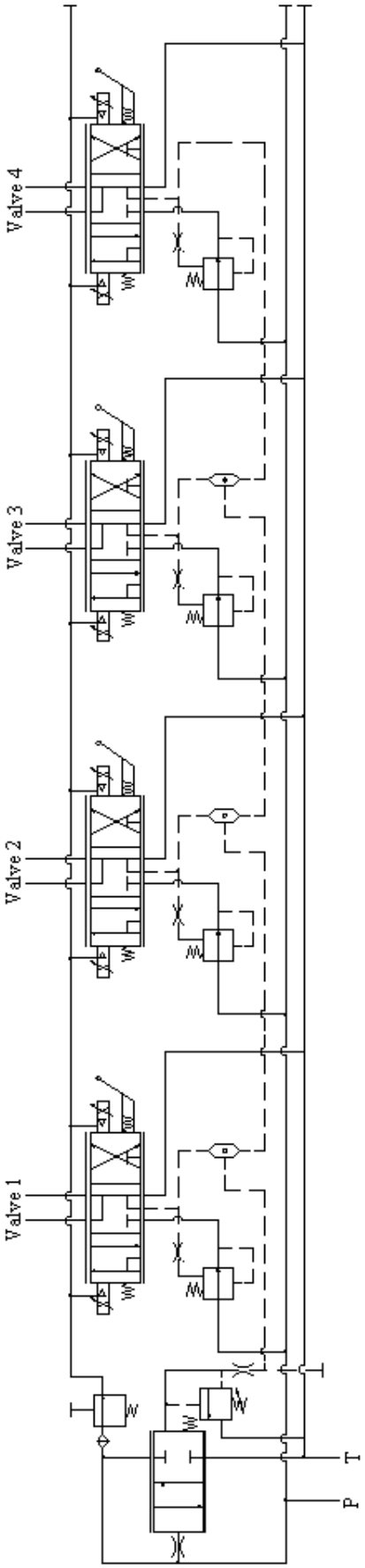

Figure B.1: Apitech VPL Series Valve (4 Sections)

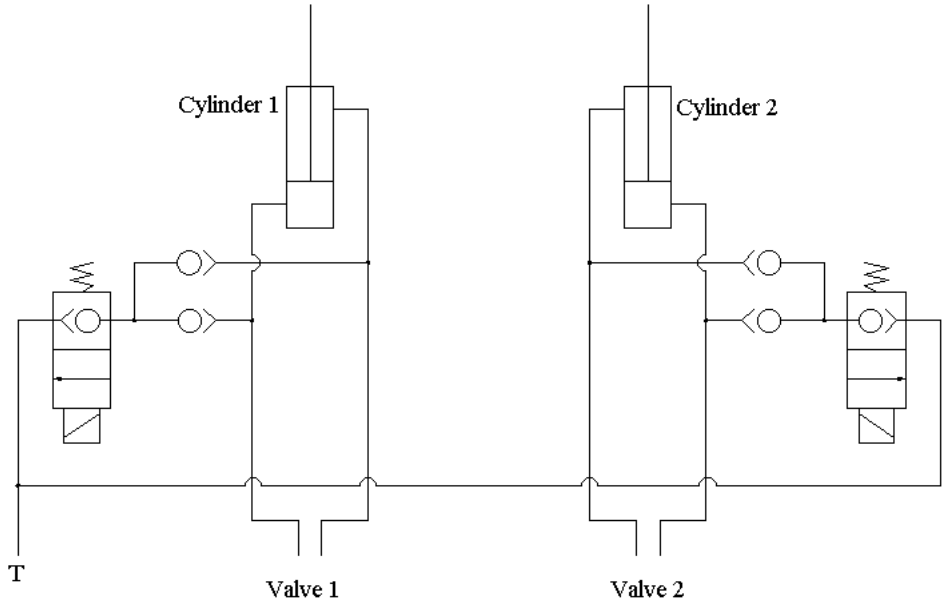

Figure B.2: Hydraulic Circuit for Swing-Arm System

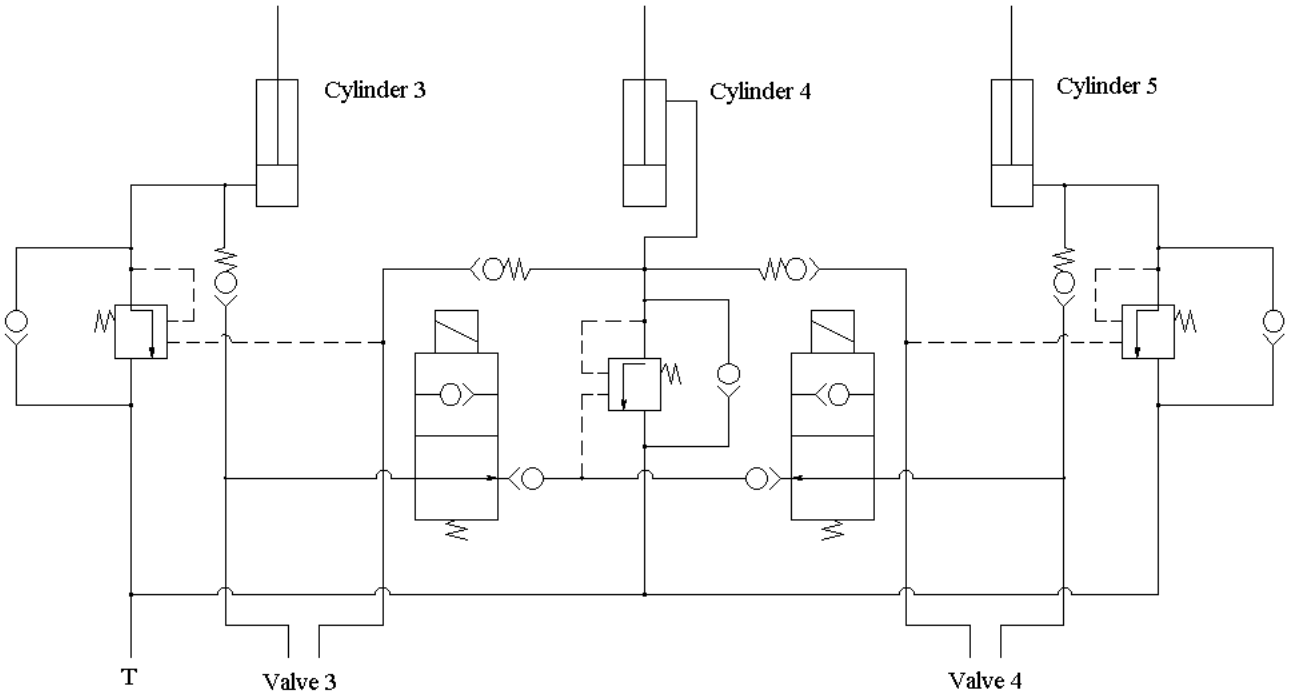

Figure B.3: Hydraulic Circuit for Mast System

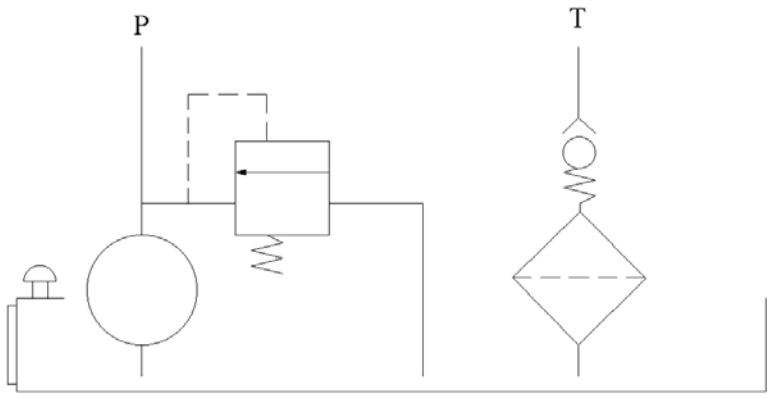

Figure B.4: Hydraulic Circuit for Pump

Appendix C

Electronic Circuits

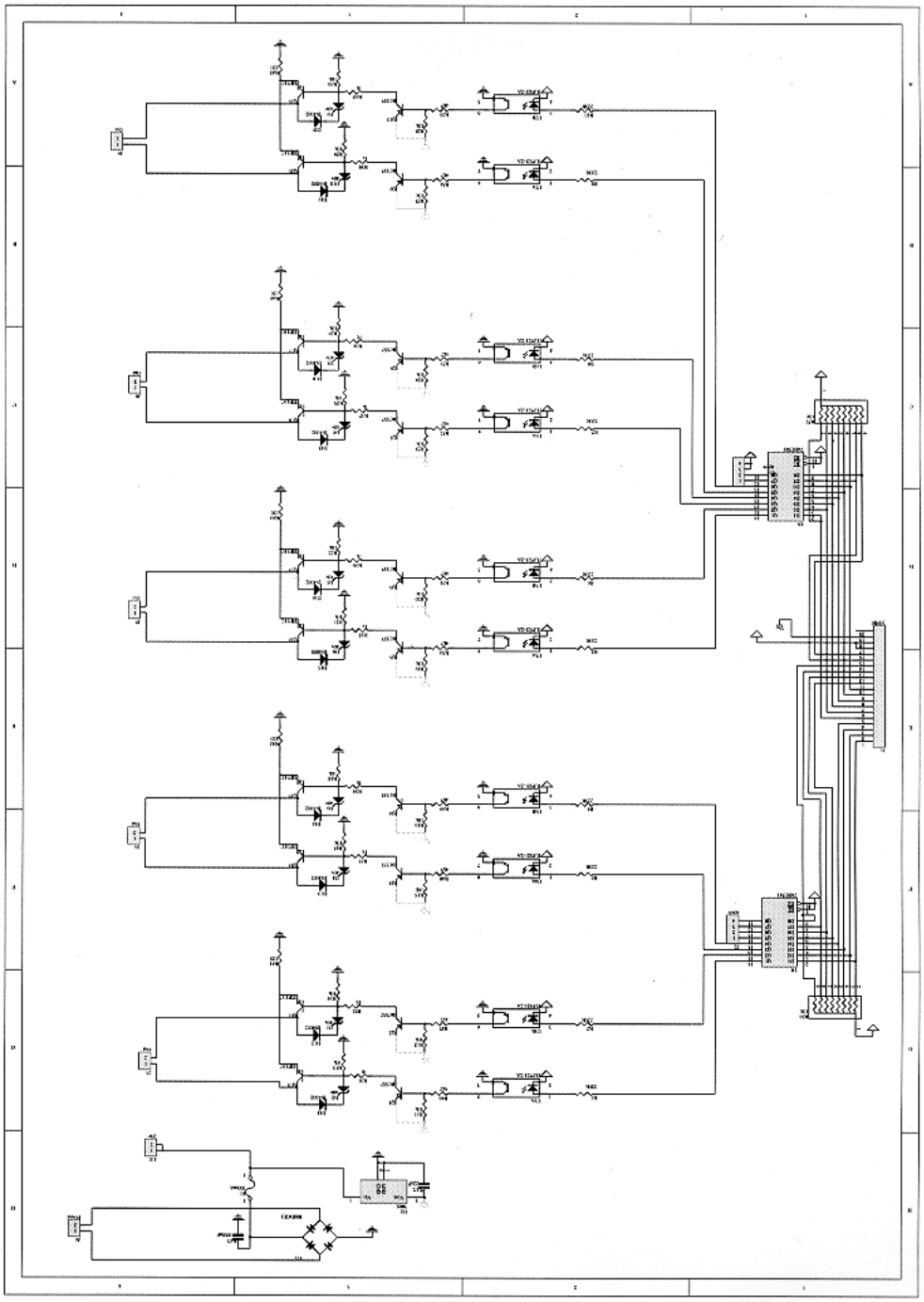

Figure C.1: PWM Amplification and Optical Isolation - Board Layout.

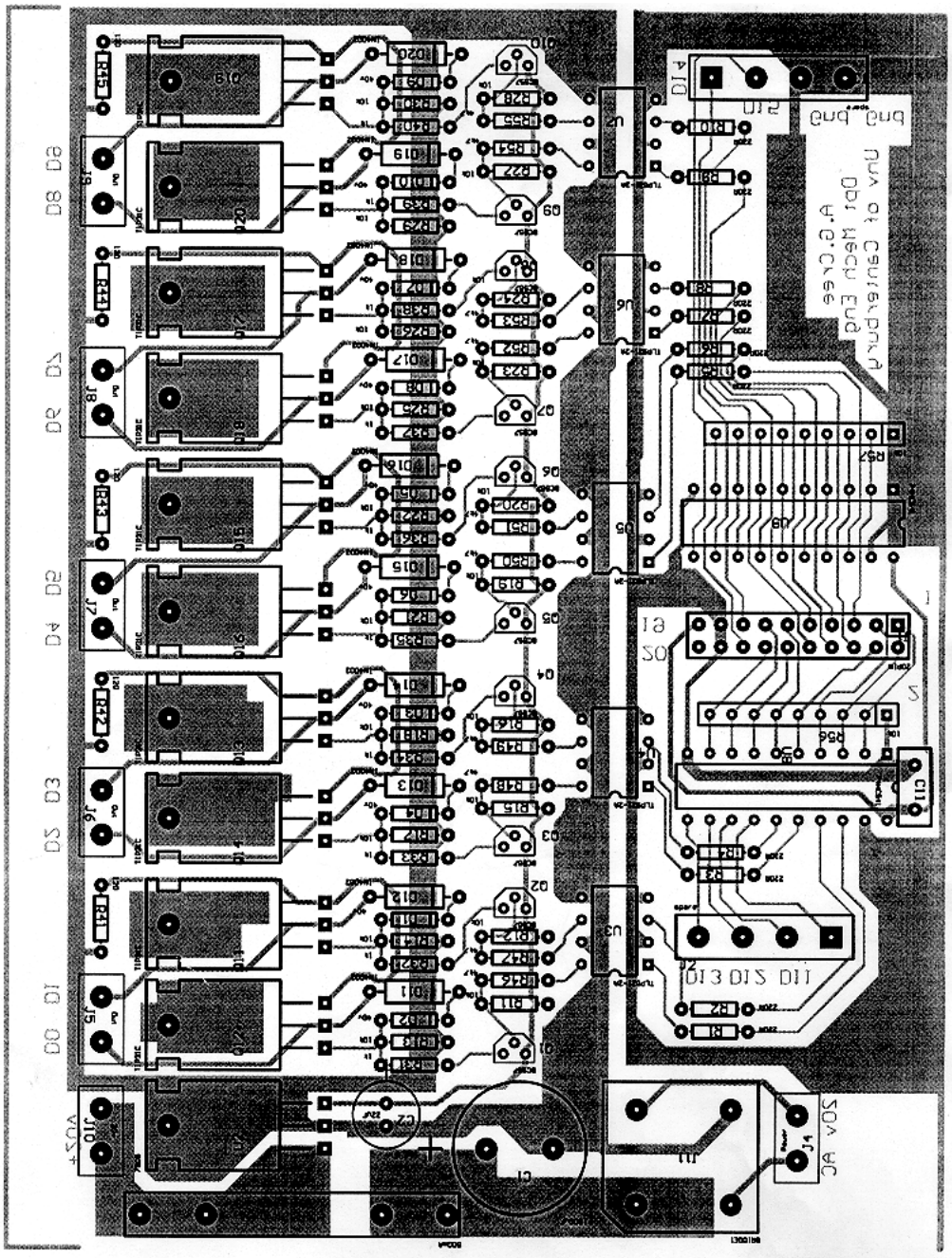

Figure C.2: PWM Amplification and Optical Isolation - Circuit Design.

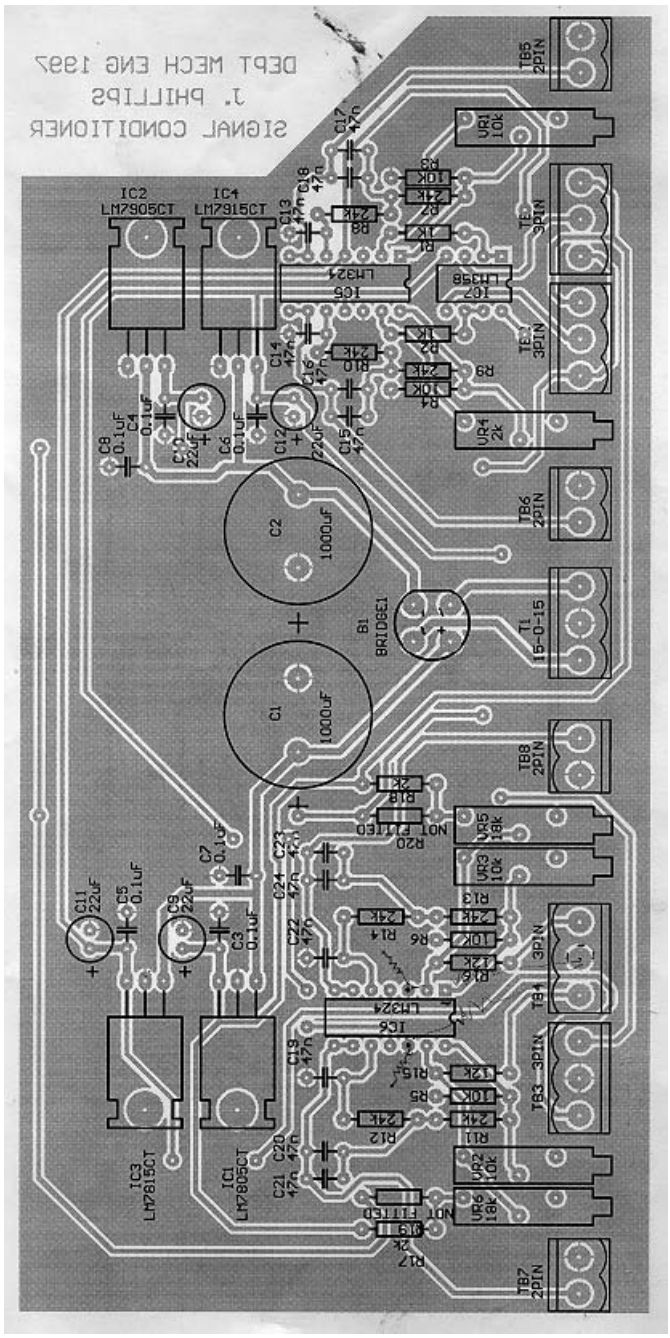

Figure C.3: Sensor Signal Conditioning - Board Layout.

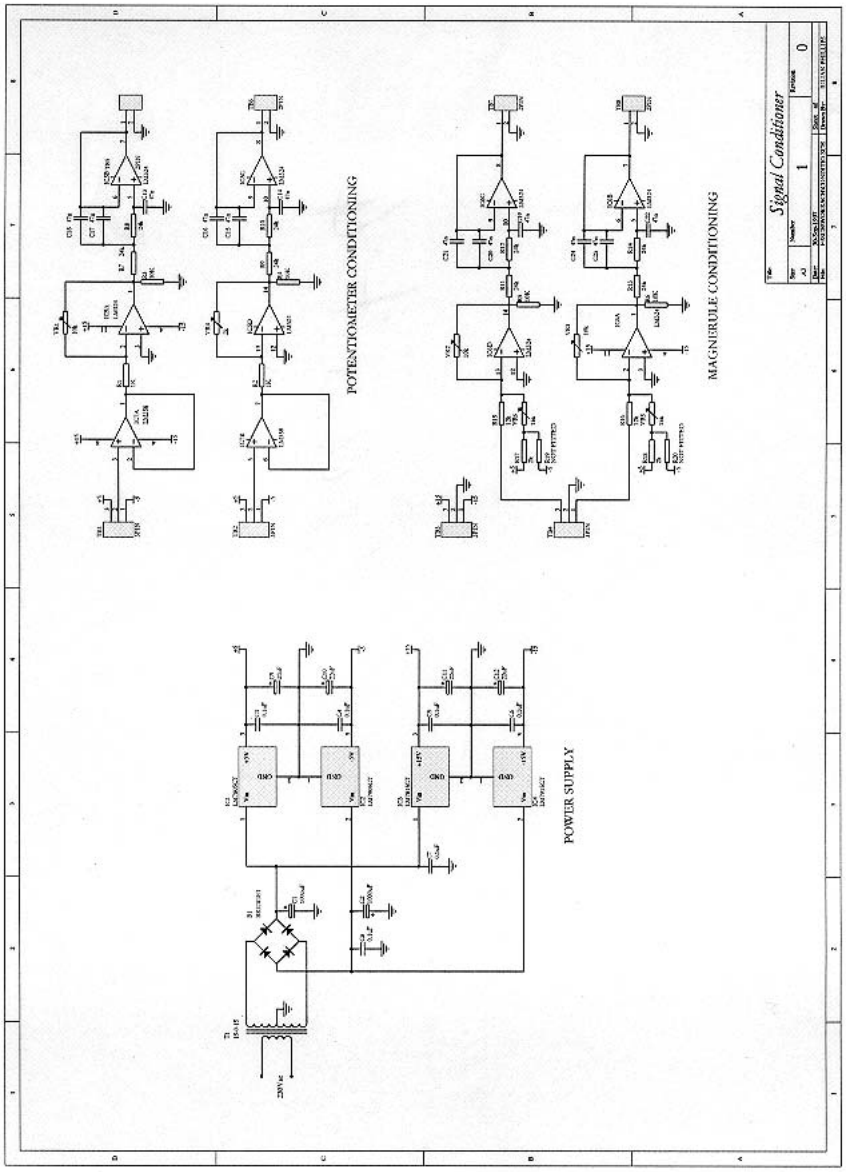

Figure C.4: Sensor Signal Conditioning - Circuit Design.

Appendix D

Digital Filter

The following MATLAB code produces a fourth order Butterworth digital filter with a cut-off frequency of 10 Hz. Digital filters are used to filter noise from the sensor inputs, and to 'round-off the corners' of the operator input command, when a step input was too harsh.

```
 [z1,p1,k1]=buttap(4);



[num1,den1]=zp2tf(z1,p1,k1);
[num2,den2]=lp2lp(num1,den1,2*pi*10);
fs=1000;
[numd,dend]=bilinear(num2,den2,fs,10);
format long f=[1 10 30 40 50 100 1000];
w=2*pi*f; hd=freqz(numd,dend,w/fs);
magd=abs(hd);
loglog(f,magd)
numd,dend
```